DEVELOPING ORDER PARAMETERS FOR ORDER-DISORDER TRANSITIONS: FROM PARTICLES TO BLOCK COPOLYMERS

A Thesis

Presented to the Faculty of the Graduate School

of Cornell University

In Partial Fulfillment of the Requirements for the Degree of

Master of Science

by

Ankita Jawahar Mukhtyar

August 2018

ABSTRACT

Block copolymers self-assemble to form a variety of different phases with highly regular patterns, depending on the microscopic ordering of molecules. Paramount to understanding and controlling this “order” is to have good “order parameters”, variables that can be used to track the changes occurring in the system as it transitions from disorder to order. Some common phases that block copolymers form include the lamellar, cylinder and gyroid network. In this paper, we use molecular dynamics to simulate the growth of these phases from an isotropic liquid. A binary nanoparticle mixture model is used that allows the simulation of systems with large enough sizes for the desired phase to nucleate and grow. We develop local order parameters based on particle symmetries and geometrical constraints that can identify and track the nucleation and growth of ordered domains along the transition pathway. We put forth a framework that could be extended towards understanding the self-assembly of other bicontinuous phases such as the double diamond or plumber’s nightmare, as well as prove useful in estimating free energy barriers and nucleation rates using rare-event sampling techniques.

BIOGRAPHICAL SKETCH

Ankita was born in Mumbai, India in 1993. She got her Bachelor of Engineering degree in Chemical Engineering from the Institute of Chemical Technology (ICT) in 2016. Her research experiences at ICT inspired her to come to the United States and pursue her Ph.D. in Chemical and Biomolecular Engineering at Cornell University in the Fall of 2016. She joined Prof. Fernando Escobedo's research group where she has been working on developing a framework to understand the order - disorder transitions taking place during block copolymer self-assembly.

ACKNOWLEDGEMENTS

I would like to thank my advisor Prof. Fernando A. Escobedo for his continued guidance and support over the last two years. His inputs and suggestions have been invaluable in helping me learn how to do research, and to navigate through the challenging aspects of this project. I would also like to thank my committee members Prof. Lynden A. Archer and Prof. Yong L. Joo for their constructive comments and feedback.

I would like to express my gratitude to members of the Escobedo group, namely Christian Nowak for teaching me how to set up my simulations when I first joined the group, Dr. Mayank Misra for being the go-to person to ask anything related to research, and Yangyang Sun and Abhishek Sharma for many helpful discussions.

Finally, I would like to thank my parents and my sister for always being just a phone call away, and for encouraging and supporting me throughout my time here.

TABLE OF CONTENTS

CHAPTER 1

Framework of Local Order Parameters

1. Introduction

There is currently a great deal of interest in functional materials (ranging from soft polymers to hard crystals) whose macroscale properties can be controlled by their microscopic structure[1]. For example, nano and micro scale colloidal particles can self-assemble into ordered lattices with interesting mechanical and optical properties[2,3]. Similarly, block copolymers (BCP) can self-assemble into structures of specific geometry with long range order[4,5], which can be used as templates to create high-surface area nanoporous materials for applications such as separation membranes[6,7], catalysts[8], solar cells[9–11] and in energy conversion and storage[12–15] devices.

Delineating the mechanism of self-assembly is necessary to be able to control the formation of a target phase of interest. Self-assembly is the process by which the polymer units spontaneously transition from a "disordered" to an "ordered" phase due to favorable thermodynamic conditions. To understand and control the kinetics of such a process we need reliable order parameters (OPs), or reaction coordinates, which are properties of the system that can quantitatively describe the relative proximity of any configuration to the disordered or the ordered basin with just a few numbers[16,17]. This idea has widely been recognized and used in various frameworks, such as in identifying floppy and stiff variables[18]. Currently, most reaction coordinates are case specific, the development of which involves significant computational effort and trial and error. The absence of a good OP can greatly hamper research efforts that attempt to simulate the kinetics of an order-disorder phase transition. For example, it took researchers many years to fully characterize the nascent structural order in the nucleation of ice[19–21] and in methane

clathrate hydrates[22,23], largely due to the lack of good OPs. This limitation is also relevant for the formation of complex self-assembled phases of BCPs, and a simple framework that can guide research in this area is still lacking.

A large number of OPs have proven to be very successful in characterizing the degree of order in crystalline and liquid crystalline phases. An example is the nematic OP (P_2) which is used to detect orientational order for systems of rod-like particles[24]. Some other methods used to detect translational order include, the smectic OP for systems of liquid crystals[25], and bond order parameters[26–28] for systems of spherical sites, also known as the Steinhardt bond order parameters. This latter method is based on rotationally invariant combinations of spherical harmonic functions, which are able to detect particular symmetries of a central particle and its neighbors in 3D space and can provide a unique signature for perfect crystal lattices. While these functions do not directly describe the structural assembly of more complex phases such as those formed by BCP, they can be adapted to describe symmetries of select morphological features in some BCP phases, as has been recently demonstrated in Ref. [62] and will be discussed later in the paper (see section 2.3.2).

One of the most commonly used methods to characterize phase formation in BCPs is the structure factor S(q). It describes how a structure scatters incident radiation due to the arrangement of its particles. When plotted as a one-dimensional function, S(q) produces a set of peaks whose ratios indicate the spacing of different planes within a structure, and these characteristic ratios can then be used to identify specific structures. Experimentally, it can be measured using small and wide-angle X-ray scattering (SWAXS). While S(q) data can easily predict the nature of the fully formed stable phase, it is too blunt a tool to capture the subtler changes that take place during the nucleation of the ordered phase from the disordered state. This

shortcoming has led to a heavy reliance on visual inspection for characterizing structures along the transition pathway, but this is not a suitable approach to compare results across independent studies. Here lies the need to develop a general metric that can easily quantify the degree of order in a system of BCPs undergoing a disorder to order transition. Further, molecular simulation methods and advances in imaging techniques now allow us to track individual particle trajectories[29–31], thereby giving us vast amounts of data which can potentially be used to model and find good OPs.

This study is a first step toward a long-term goal of developing an all-purpose analysis technique, akin to those used in the computer science field of shape matching or pattern recognition (PR). Such a technique would offer a potentially powerful solution to the problem of creating general structural metrics for complex systems. Pattern recognition is commonly used in finger print[32] and facial recognition[33] techniques to identify good matches from a sample set to a reference structure. The advantage of PR-based methods lies in their potential applicability to different systems, and their ability to interpret results that may lead to better insights into the structure of a material. While much progress remains to be done before an ideal structure characterization technique is developed, in this paper we put forward OPs that recognize simple local patterns in BCP phases through the construction of appropriate local correlation functions.

1.1 Nucleation of Ordered Phases in Block Copolymers

The ability to control the formation of ordered mesophases in BCPs entails an understanding of its ordering mechanism; that is, of the factors that determine its nucleation and growth rate and the free energy landscape that it has to negotiate. Early experimental studies found the formation of an ordered lattice in BCPs to be unusual, because it involved two distinct processes[34–36]: a fast process of microphase separation followed by a slow aligning process that

led to the development of long-range order. Theoretical studies reported unusually small nucleation barriers for the disorder to lamellar transition, characterizing them as being only weakly first order[37,38]. Later studies on transitions between disordered and lamellar[39,40] or disordered and cylinder phases[41–43] revealed the presence of anisotropic droplets of the ordered phase that had indeed nucleated from the disordered phase after an incubation time. This was also confirmed using classical nucleation theory for the disorder to lamellar transition[44].

From a computational perspective, disorder to lamellar and disorder to cylinder transitions have been studied using various techniques such as field-theoretic simulations[45,46], on-lattice[47–49] and off-lattice[50–52] Monte Carlo, dissipative particle dynamics[53–55] and molecular dynamics[56,57]. While the results from these computational studies do provide an insight into the mechanism of ordering, a quantitative description of the specific kinetic pathway for disorder-order transitions is still lacking. Carilli et al.[58] attempted to fill this gap for the disorder to lamellar transition using the renormalized Landau-Brazovskii model, and estimated the free energy barriers and critical nucleus size for the transition. However, they found their estimates for critical nucleus size to depend greatly on their predicted order – disorder transition (ODT), such that even a minor error in ODT resulted in a large error in critical nucleus size. They further confirmed the need for a local OP that can effectively track the nucleation process and be used as a metric in techniques like metadynamics[59] or umbrella sampling[60,61], to extract free energy barriers. We attempt to fill this gap in this paper, by putting forth local OPs that can effectively track order-disorder transitions in BCP-like phases.

Recently, Kumar and Molinero[62] demonstrated the use of bond orientational order parameters[28] to investigate the nucleation of lamellar, cylinder and gyroid phase in a binary mixture of nanoparticles (henceforth referred to as the KM model) that produce BCP-like

phases[63]. While their OPs were able to identify and track the growth of the phases, they do not have a simple physical interpretation and it is still unclear whether these OPs could be extended to more realistic BCP models.

In the present work, we use the KM model mentioned previously, to observe the disorder to order transitions in three of the BCP phases (lamellar, cylinder and alternating gyroid). Critical to observing the formation, growth and alignment of nuclei in the BCP matrix, is the ability to simulate a system that is large enough to capture these changes. Most molecular dynamic simulations of BCPs are limited by relatively small system sizes, i.e., where only one or a few unit cells of the repeating motif appear, which precludes the appropriate description of the different length scales involved in nucleation (that could easily exceed the size of the simulation box). The KM model overcomes that issue by allowing the use of very large system sizes, where numerous unit cells of the morphology can be formed, hence serving as a good platform to test and develop OPs that could be used for realistic polymer models. Accordingly, we developed a local OP that captures the inherent geometries of the lamellar, cylinder and alternating gyroid phases, through a set of physically intuitive parameters (related to the axes of symmetry for the lamellar and cylinder phases). For the alternating gyroid that has a more complex structure, our OP involves identification of the smallest repeating unit, or a unit cell, due to its symmetries extending beyond its immediate neighborhood. We expect that these OPs will lay the framework for further understanding the kinetic pathways in disorder – order transitions of BCPs.

2. Method

2.1 KM Model Description

The simulations involve binary nanoparticles (A and B), that interact through a simple, short-range isotropic potential (a two-body Stillinger-Weber potential), characterized by energy

parameters ε_{ij}, size parameters σ_{ij} and the mole fraction of A, X_A. Further details of this KM model are given in the paper by Kumar and Molinero[63]. A key feature of the model that leads to the formation of BCP-like phases is that the attraction between different particle types is stronger than that between same particle types ($\varepsilon_{AB} / \varepsilon_{AA} > 1$). However, different particle types cannot get as close as particles of the same type ($\sigma_{AB} / \sigma_{AA} > 1$), which causes the latter to come closer. This frustration leads to the formation of the different phases. Indeed, while the potential energy favors the formation of AB pairs, microphase segregation arises to minimize the larger excluded volume that AB pairs create (compared to that for AA and BB pairs). Throughout all the simulations we keep $\sigma_{AA} = \sigma_{BB} = 1$, and $\varepsilon_{AA} = \varepsilon_{BB} = 1.0$ kcal mol^{-1}. The values of $\varepsilon_{AB}/\varepsilon_{AA}$ (X_A) vary as 1.1 (0.5), 1.7 (0.775) and 2.25 (0.5) for lamellar, cylinder and alternating gyroid respectively. σ_{AB} was kept at 1.15 for lamellar and cylinder, and 1.02 for the alternating gyroid. These values were decided in accordance with the phase diagram by Kumar and Molinero[63]. Since the phase boundaries are only approximate we cannot estimate the degree of supersaturation (DSS) quantitatively, however we know qualitatively how far we are from the phase boundary in each case. The lamellar phase is reported to have almost no nucleation barrier up to 8% below its melting temperature[62], or in this case the ε_{AB} value at the phase boundary. The cylinder phase also exhibits a similar trend. Since our simulation conditions lie well within the stability regions of both, i.e., large DSS, we expectedly find the disorder-to-order transition to be nearly barrier-less and proceed via a spinodal-decomposition-like process. However in the case of gyroid, nucleation rates are generally low[64,65] and hence despite being away from the phase boundary we find the isotropic phase to be a long-lived metastable phase and the ordering transition to occur via nucleation.

2.2 Simulation Details

All our MD simulations were performed using the LAMMPS software[66]. We start with an isotropic KM mixture of 13824 particles in a random initial configuration. All parameters except for the distances are reported in real units. The mixture is simulated in an NPT ensemble at a T = 300 K and P = 0 atm with periodic boundary conditions in all three directions. Forces are integrated using the Velocity Verlet algorithm with a time step $\Delta t = 0.05$ fs. Temperature and pressure are controlled with the Nose-Hover thermostat and barostat with time constants $500\Delta t$ and $2500\Delta t$, respectively. Simulations are performed until the stable phase at that composition forms and fills the entire box.

2.3 Order Parameters (OPs)

Our OPs aim to capture key features of the local geometry of a phase morphology by identifying symmetries that are unique to that phase. For the two-dimensional phases (lamellar and cylinder) this simply involves identifying the principal axis of symmetry (normal vector of the lamella plane or direction vector of the cylinder axis). The alternating gyroid network is characterized by $I4_132$ symmetry[67–69], which can be identified using appropriate bond-orientation order parameters[28] of spherical harmonics (a set of complex vectors). As will be explained in greater detail in Sections 2.3.1 and 2.3.2, we associate a set of phase-signature vectors to each particle in the simulation. The dot product of neighboring vector pairs then tells us the extent of their correlation, a higher value indicating stronger correlation. We use this definition to differentiate between the "disordered" and "ordered" particles, after which a clustering algorithm is used to group all the "solid-like" particles together.

2.3.1 2-D Phases (Lamellar and Cylinder)

The binary nanoparticle mixture model gives us lamellar and cylinder phases with feature sizes of the order of a single particle (See Fig. 1). This simplifies many of the calculations necessary to characterize these phases, and hence serves as a good model to develop and test model OPs.

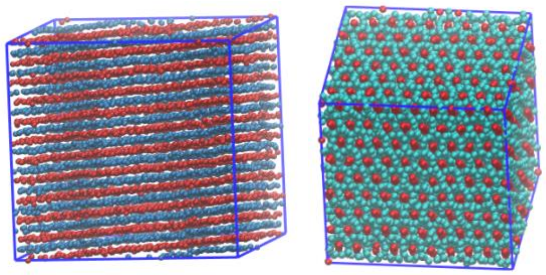

Figure 1: Left: Lamellar phase shown by the red and blue layers, each layer one particle thick. Right: Cylinder phase with the minority component shown in red. Individual cylinders one particle thick.

For the Lamellar Phase

For a given particle, a cutoff radius (r_c) is defined approximately as the inter-particle distance (r) where the first minimum of the radial distribution function g(r) occurs. Particles of the same type as the central particle and within the cutoff radius are identified as nearest neighbors. In the lamellar phase, particles stack up in layers and so each layer has an axis of symmetry that can be found by fitting a plane to particles in the cutoff and identifying the direction of the normal vector. This is done using singular value decomposition to determine the smallest eigenvalue, which represents the direction of least spread, in this case the normal vector to the plane. Once normalized to a unit length, this normal unit vector will be henceforth denoted as lamella-signature "LS" vector. The process is repeated until each particle in the simulation has its own LS vector. To quantify the degree of alignment, the angle between the LS vectors of neighboring particles is measured. It is worth mentioning, that while in this case a simple dot product of any two LS vectors $\mathbf{n}_i$ and $\mathbf{n}_j$ suffices as an indicator of the extent of correlation, an alternate approach could involve computing the Legendre polynomial P_2 ($\mathbf{n}_i \cdot \mathbf{n}_j$) for such vectors, which

would also give a value of 1 for complete alignment, as pertaining to the ordered state. In a perfectly ordered lamellar phase all particles lie in parallel planes, and correspondingly all their LS vectors should align in the same direction (or at 180° to each other, see Fig. 2). This metric is used to determine if a particle has at least 4 neighbors with which its LS vector aligns, after which it is marked as "lamellar-like". This is repeated for all particles in the simulation until the "lamellar-like" particles have been identified. They are then clustered depending on their

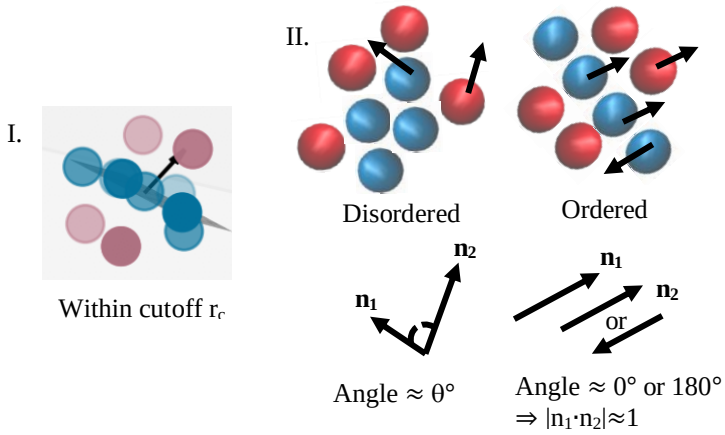

Figure 2: Depiction of steps to find Lamellar signature (LS) vectors and OP: I = Fitting a plane to same atom types and find normal or LS vector; II = Finding the angle between neighboring LS vectors.

proximity to one another using the nearest neighbor cutoff r_c. This method allows us to track the growth of the ordered "lamellar-like" particles with time. As seen in Fig. 3, the scatter plot of the LS vectors of all particles on a unit sphere surface show very distinct patterns for a disordered

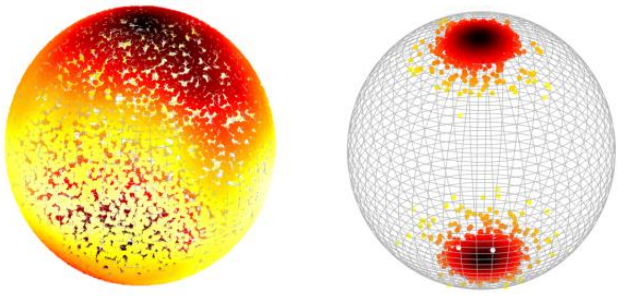

Figure 3: Distribution of the lamella-signature (LS) vectors of all particles on a sphere, at X_A=0.5, ε_{AB} = 1.1 kcal/mol, σ_{AB} = 1.15 and T=300K, P=0 atm. In the fully ordered state we can see that the LS vectors have aligned in one direction. Color gradient is an indicator of the local density in that region.

initial phase and for the fully ordered lamella phase.

For the Cylinder Phase

The process is similar to that followed for the lamellar phase. Here, particles of the minority component (shown in red in Fig. 4) arrange themselves in a line. Their axis of symmetry, or direction vector, can be found by fitting a line to all minority components identified within the

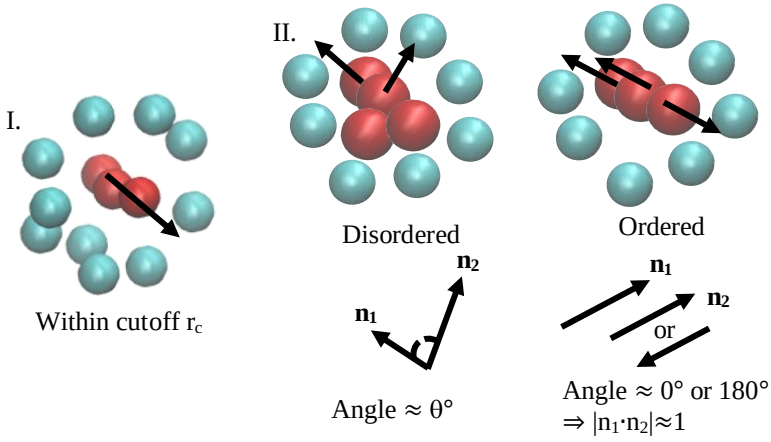

Figure 4: Depiction of steps to find cylinder signature (CS) vectors and OP:
I. Fit a line to same atom types and find direction or CS vector.
II. Find the angle between neighboring CS vectors

cutoff. This is done using again singular value decomposition to determine the largest eigenvalue, which represents the direction of maximum spread, in this case the direction vector of the cylinder, which once normalized to a unit length will be denoted as the cylinder-signature "CS" vector. The process is repeated until each particle of the minority component has its own CS vector. To quantify the degree of alignment, the angle between the CS vectors of neighboring particles is measured. In a perfectly ordered cylinder phase all particles lie in parallel lines, and correspondingly all their direction vectors should align in the same direction (or at 180° to each other, see Fig. 4). This metric is used to determine if a particle has at least 2 neighbors with which its CS vector aligns, after which it is marked as "cylinder-like". This is repeated for all particles in the simulation until the "cylinder-like" particles have been identified. They are then clustered depending on their proximity to one another using the nearest neighbor cutoff r_c. This method allows us to track the growth of the ordered "cylinder-like" particles with time. The CS vectors of the minority component particles plotted on a unit sphere surface clearly show a

change in pattern from a uniform distribution in the isotropic phase to a bipolar distribution in the fully ordered cylinder phase (see Fig. 5).

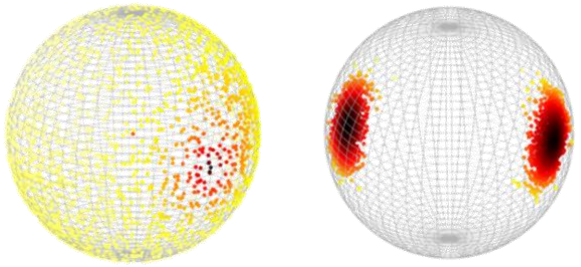

Disordered Ordered

Figure 5: Distribution of unit direction vectors or cylinder-signature (CS) vectors of the minority component on a sphere, for the cylinder phase at X_A=0.775, ε_{AB} = 1.7 kcal/mol, σ_{AB} = 1.15 and T=300K, P=0 atm. In the fully ordered state we can see the CS vectors have aligned in one direction. The color gradient is an indicator of the local density.

2.3.2 Alternating Gyroid Network

The alternating gyroid network ($I4_132$ space group) is a continuous, triply periodic cubic morphology that has gained significant interest due to its geometric characteristics and inherent chirality[70,71] not observed in other similar morphologies. It is made up of two intertwined but chemically distinct single networks of equal volume fractions (See Fig. 6), similar to those found

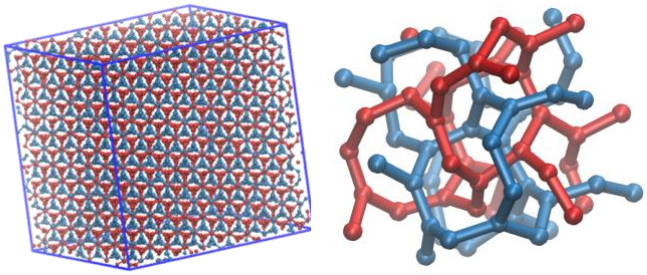

Figure 6: Left: Fully formed alternating gyroid (two distinct networks shown in red and blue). **Right**: A zoomed-in view of the network structure where every particle act as a node connected by struts to three neighboring particles.

in nature in the colored wings of certain butterfly species[69]. To the best of our knowledge, while the single gyroid (consisting of only one network) has been shown to form in self consistent field theory studies of order-order transitions in triblock copolymers[72], the direct nucleation of the alternating gyroid from disorder has not been reported. It was observed by Kumar and Molinero, in their paper on the KM model[63], however the nucleation process leading to formation of the phase was not described. Here we develop an OP that is able to detect the growth of the

alternating gyroid from an isotropic liquid. Each network is considered separately.

First, a list of neighbors is determined for each particle consisting of all particles of the same type found within a radial distance r_c of particle *i*. Unlike the previous phases where the symmetry of the basic repeating motif could be described by a single vector, in this case multiple vectors are needed as the basic repeat unit is a 3D unit cell. A suitable way to define the relative orientation of multiple (rotationally invariant) vectors is through the Steinhardt OPs. Accordingly, the r_c is chosen here to be a value that is large enough to include neighbors beyond the first coordination shell (up to the third g(r) peak). The total number of neighbors for every particle, denoted by $N_b(i)$, is then used to calculate the bond orientational OP[73] $q_{l,m}(i)$:

$$q_{l,m}(i) = \frac{1}{N_b(i)} \sum_{j=1}^{l} Y_{l,m}(\theta_{i,j}, \phi_{i,j}) \qquad (1)$$

where $Y_{l,m}(\theta_{i,j}, \phi_{i,j})$ are the spherical harmonics, $m \in [-l, l]$ and $\theta_{i,j}$ and $\phi_{i,j}$ are the polar and azimuthal angles of $r_{i,j}$ (distance vector between particles i and j) and r_i (position vector of particle i). The symmetry index l for the bond orientational OP is chosen to be 6 since q_6 works well for BCC lattices[61], and we know from the $I4_132$ space group that nodes of the alternating gyroid are situated on a BCC lattice. We can define $q_6(i)$ as a "vector" (for particle *i*) having $2l+1 = 13$ components $q_{6,m}(i)$ (one for each m value) and will be denoted as the Gyroid-Signature "GS" vector of particle *i*. To find the correlation between two neighboring particles *i* and *j* , we calculate the appropriate "dot" product[73] for the GS vectors defined by:

$$d_l(i,j) = \frac{\sum_{m=-l}^{l} q_{l,m}(i) q_{l,m}^*(j)}{\left(\sum_{m=-l}^{l} |q_{l,m}(i)|^2\right)^{1/2} \left(\sum_{m=-l}^{l} |q_{l,m}(j)|^2\right)^{1/2}} \qquad (2)$$

Where * indicates the complex conjugate. The correlation function is computed for all pairs of neighboring particles in the system and the corresponding histograms can be seen in Fig. 7(a-d) below for both the ordered and disordered phases.

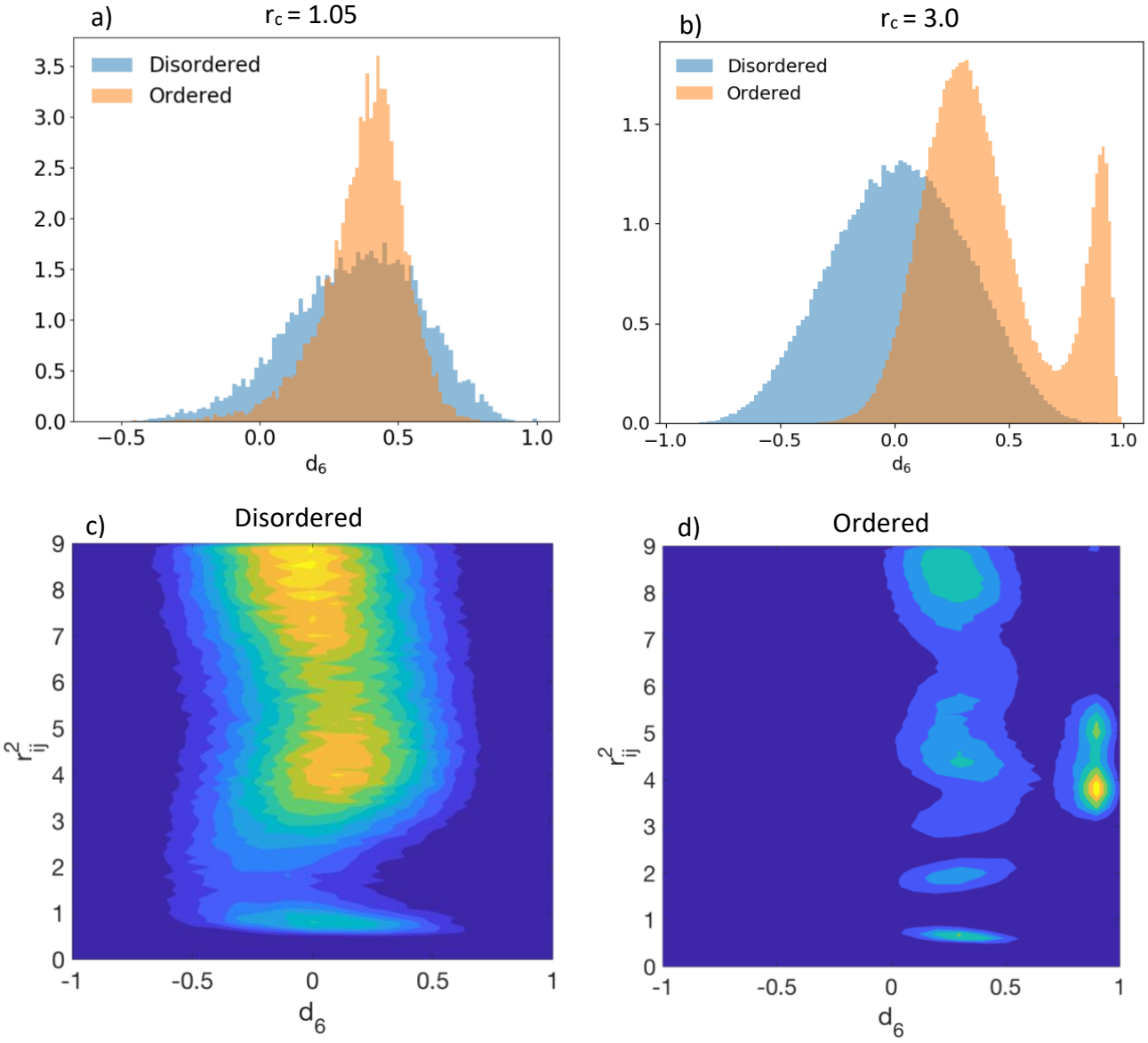

Figure 7: Histograms of the correlation function d_6 for the ordered and disordered phases of the alternating gyroid at X_A=0.5, ε_{AB} = 2.25 kcal/mol, σ_{AB} = 1.02 and T = 300K, P = 0 atm. a) For a radial distance cutoff r_c = 1.05, there is no significant difference between the two. b) For r_c = 3.0 there is a distinct second peak at $d_6 > 0.75$ for the ordered phase. c-d) Two-dimensional histograms of d_6 with r_{ij}^2 at r_c = 3.0, showing the existence of a second peak for $d_6 > 0.75$ and $3 < r_{ij}^2 < 6$.

In Fig 7a, r_c was set as 1.05, which included neighbors within the first g(r) peak only. It can be seen that there is no significant difference in the correlation functions of the ordered and disordered phases, suggesting the need for a larger r_c that includes more neighbors. Indeed, when the cutoff is increased to r_c = 3.0 (used in all further calculations), we see the appearance of a

strong second peak for the ordered phase above a certain d_6 value (see Fig. 7b). This d_6 value is taken as a threshold to differentiate between ordered and disordered particles, which in this case is equal to 0.75. Fig. 7c and 7d show the variation in d_6 with r_{ij}^2 (center to center distance between neighboring particles) at $r_c = 3.0$ for the disordered and ordered phases, respectively. A second peak can be seen clearly in the ordered case, for $d_6 > 0.75$ and $3 < r_{ij}^2 < 6$, confirming the expectation that symmetries of the alternating gyroid phase extend beyond its immediate neighborhood. This allows us to define two neighboring particles *i* and *j* to be connected if their dot product d_6 exceeds 0.75. By using this definition, we can effectively identify all the ordered particles, however we need to check how many such connections exist per particle for both the ordered and disordered phases. Fig. 8 shows the distribution function for the number of connections per particle, denoted by ξ. From this, we can define another threshold ξ_c to unambiguously identify "gyroid-like" particles so that for $\xi(i) > \xi_c$ particle *i* is considered "gyroid-like", while for $\xi(i) \leq \xi_c$ it is considered to be "liquid-like". Based on the distributions shown in Fig. 8, ξ_c was set as 8. This selection process is carried out until all the "gyroid-like" particles have been identified. These particles are then clustered depending on their spatial

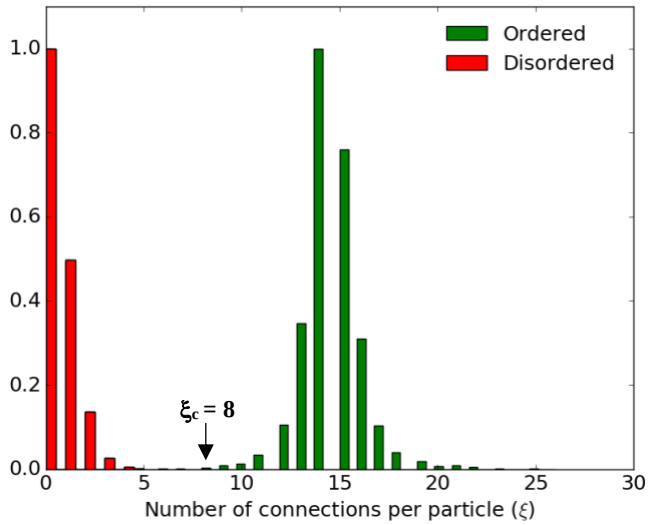

Figure 8: Distribution function of the number of connections per particle. Two particles are considered connected if their correlation function d_6 is greater than 0.75.

proximity to one another, using the nearest neighbor cutoff r_c. This method was used to track the nucleation and growth of the alternating gyroid phase with time.

2.3.3 Comparison to alternative OPs

One of the key features of our OP is its ability to detect growing nuclei by only considering neighbors in the first shell for lamellar and cylinder motifs. This is different from the OP developed by Kumar and Molinero[62], where they had to account for neighbors beyond the first shell in order to detect the lamellar and cylinders motifs in the isotropic liquid. The need to account for farther neighbors in case of the alternating gyroid network can be explained by its unit cell structure, which consists of 8 nodes from each network[68]. This also provides an understanding for why we get a ξ_c value of 8 from Fig. 8, indicating that unit cell formation is a critical step toward gyroid structure identification. We implemented the OP of Kumar and Molinero[62] which was shown to identify the double gyroid phase for our alternating gyroid system to see if it could effectively track the nucleation. This involved a calculation of the

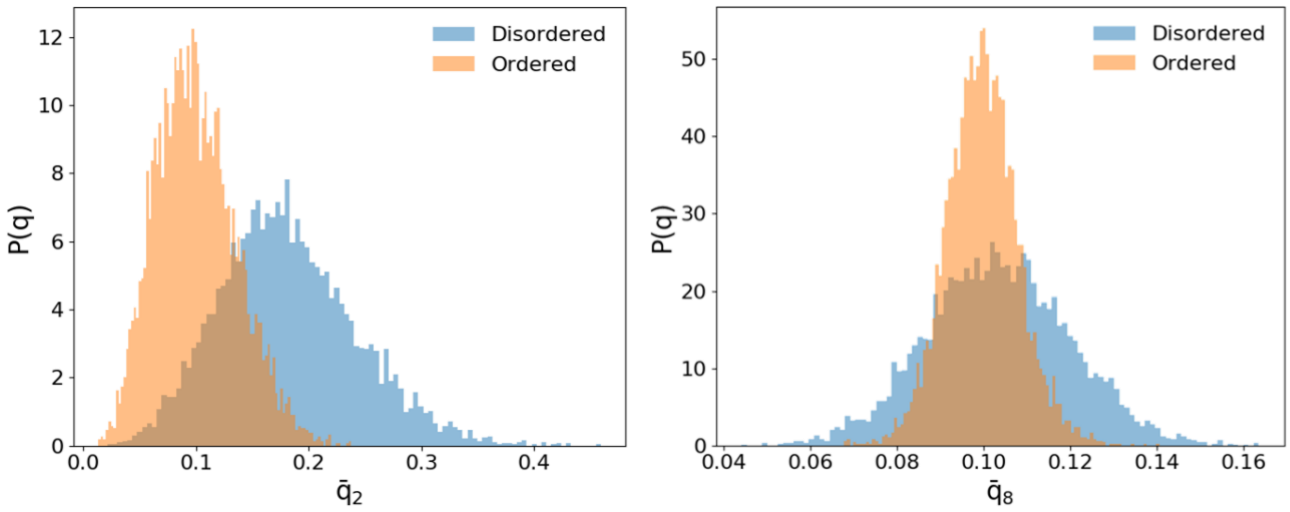

Figure 9: Distribution of OP $\bar{q}_2$ and $\bar{q}_8$ for the alternating gyroid system at X_A= 0.5, ε_{AB} = 2.25 kcal/mol, σ_{AB} = 1.02 and T = 300K, P = 0 atm. Nearest neighbor cutoffs are 1.91 and 3.39 respectively. The ordered and disordered distributions overlap significantly suggesting the need for a more effective OP.

average bond order parameters $\bar{q}_2$ and $\bar{q}_8$ for each particle using the optimized nearest neighbor cutoffs of 1.91 and 3.39 respectively, as given in Ref. [62] phase. As can be seen in Fig. 9, the distributions for the ordered and disordered phases overlap significantly and hence would not be able to correctly distinguish the ordered particles from the disordered. This suggests that their chosen OPs cannot be directly applied to study other systems, even those having similar morphology, and likely need to be re-calibrated (perhaps by a different neighbor cutoff) before they can be effective. In contrast, we think our OP for the alternating gyroid could be extended to work for many similar network morphologies that lie on a cubic lattice.

3. Results and Discussions

3.1 Formation of the Lamellar Phase

The growth of the lamellar phase at 300 K, X_A = 0.5 and ε_{AB} = 1.1 proceeds via spinodal decomposition, seen through the alignment and coarsening of multiple ordered domains into a

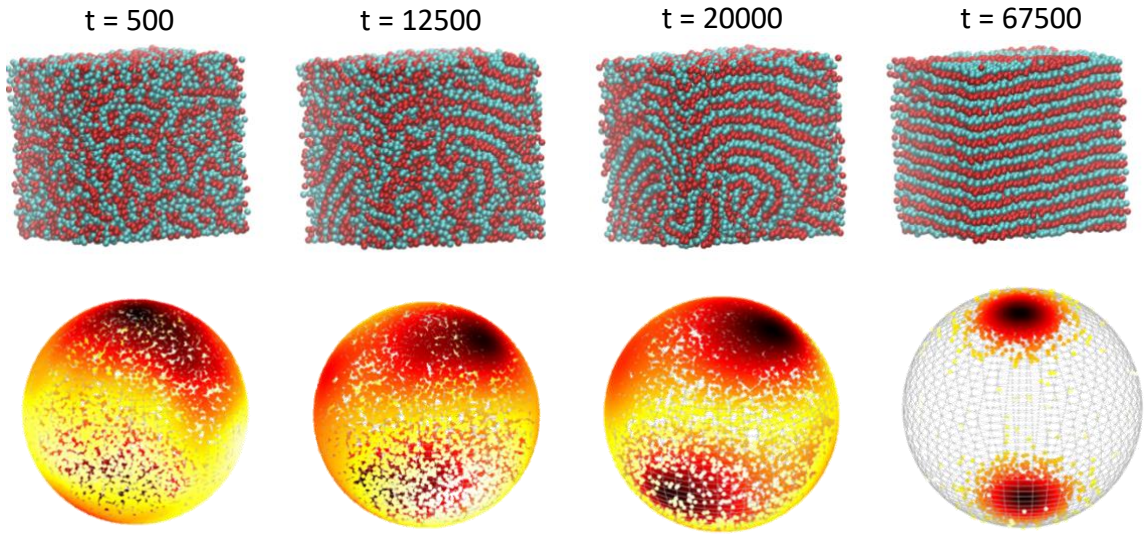

Figure 10: Growth of the lamellar phase at X_A=0.5, ε_{AB} = 1.1 kcal/mol, σ_{AB} = 1.15, T = 300 K and P = 0 atm. **Top:** Bulk simulation snapshots where red and blue correspond to the two components of the binary nanoparticle mixture. Formation of multiple layered domains that coarsen and align with time can be seen. **Bottom:** Spherical distribution plots showing the LS vectors of all particles beginning to align as the layers start to straighten. Color gradient is an indicator of the local density. Time units are in fs.

single domain (see Fig. 10). The ordering is spontaneous and occurs through multiple misaligned nuclei that form and grow simultaneously at multiple locations in the box (see Fig. 11). Despite the initial presence of multiple lamellar "grains", these are eventually able to realign to produce a final structure with no grain boundaries or defects. These nuclei are identified using the lamellar OP mentioned earlier, which helps us quantitatively track the disorder to order transition.

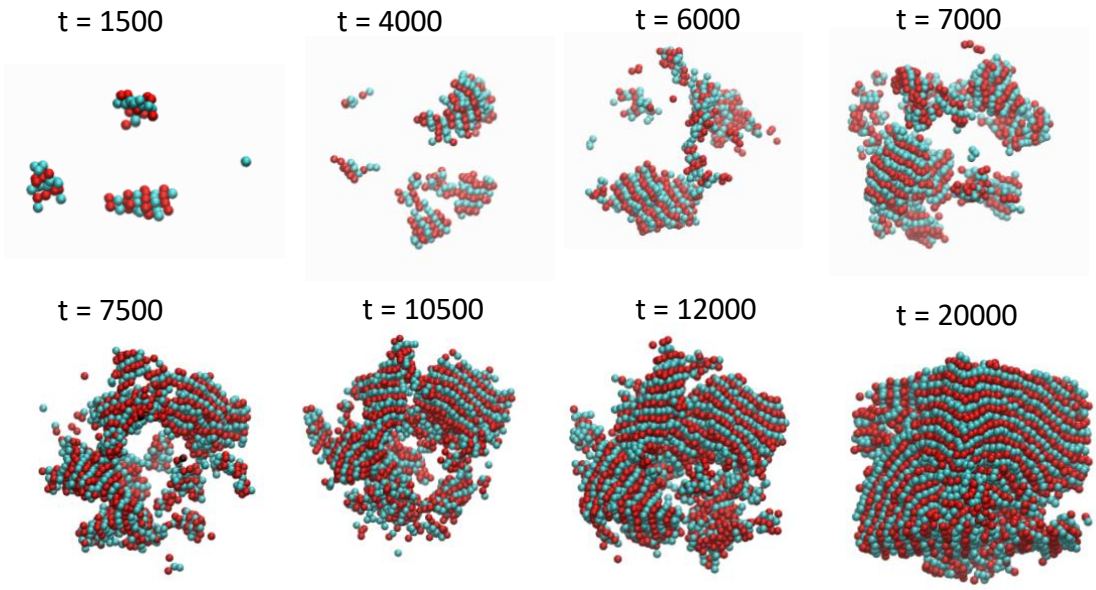

Figure 11: Cluster identification using lamellar order parameter. The 4 largest ordered clusters present in the simulation box are shown at different times (not all clusters shown for clarity). Red and blue correspond to the two components of the binary nanoparticle mixture. It can be seen that the clusters are initially oriented in random directions but then gradually coarsen and align. Time units are in fs.

3.2 Formation of the Cylinder Phase

The growth of the cylinder phase from a disordered state at T = 300 K, $X_A = 0.775$ and $\varepsilon_{AB} = 1.7$ also proceeds via spinodal decomposition. This can be seen in Fig. 12 through the multiple domains displaying cylindrical order that are found to be present but are not aligned in the same direction. Our OP detects these multiple clusters which can be seen in Fig. 13 and correspond to the bulk simulation snapshots shown in Fig. 12. Over time, the different ordered grains come together and begin to straighten out until they form the stable cylindrical phase. This

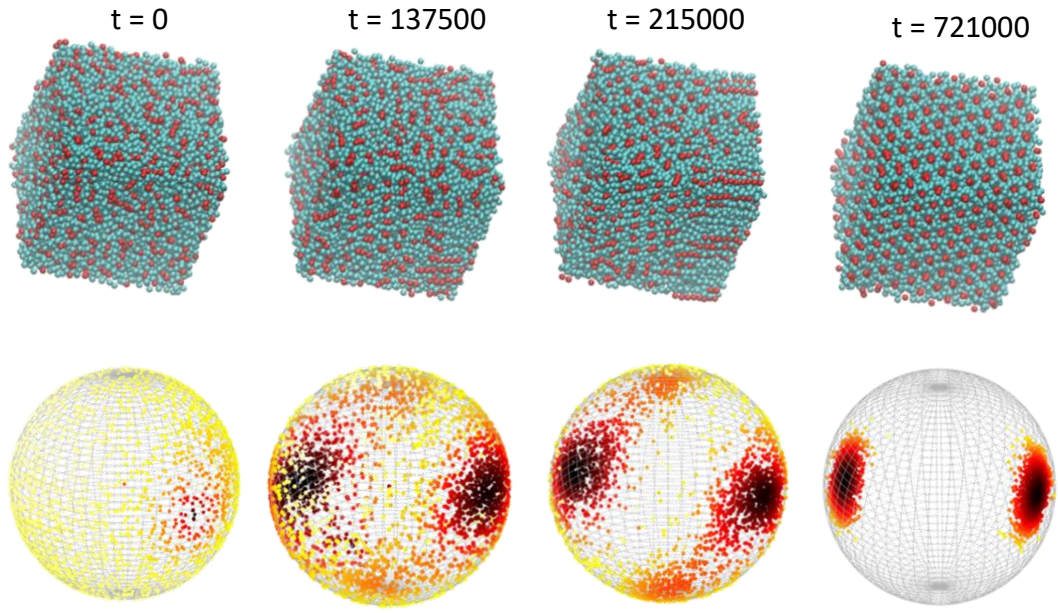

Figure 12: Growth of the cylinder phase at $X_A = 0.775$, $\varepsilon_{AB} = 1.7$ kcal/mol, $\sigma_{AB} = 1.15$, T = 300K and P = 0 atm. **Top:** Bulk simulation snapshots where red and blue correspond to the two components of the binary nanoparticle mixture. The formation of multiple differently oriented cylinders that coarsen and align with time can be seen. **Bottom:** Spherical distribution plots showing the CS vectors of all particles beginning to align as the cylinders start to straighten. Color gradient is an indicator of the local density. Time units are in fs.

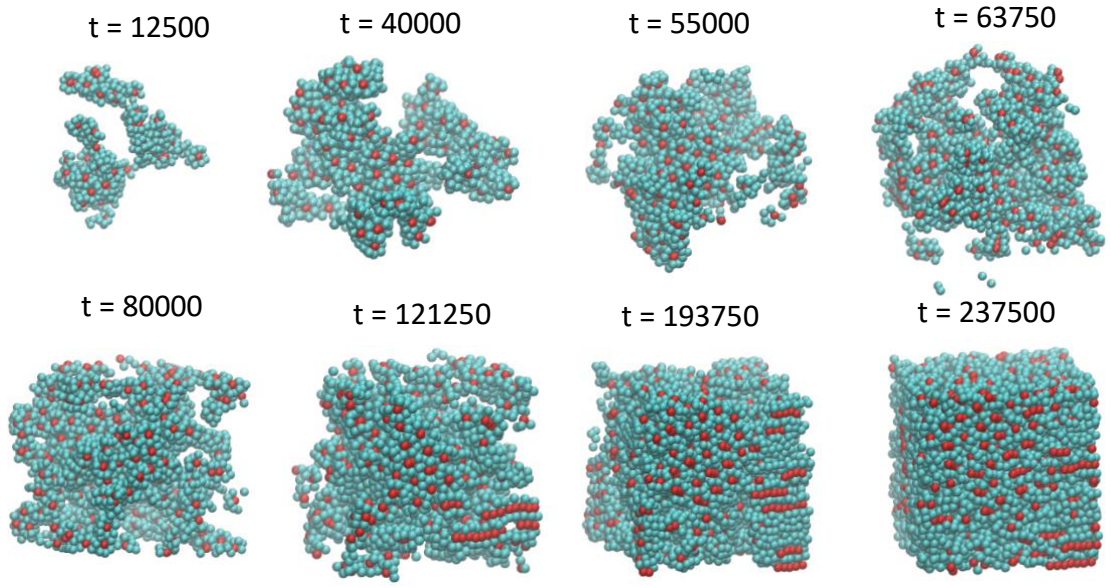

Figure 13: Cluster identification using cylinder order parameter. The 4 largest ordered clusters present in the simulation box are shown at different times (not all clusters are shown for clarity). Red and blue correspond to the two components of the binary nanoparticle mixture. It can be seen that the clusters are initially oriented in random directions but then coarsen and align over time. Time units are in fs.

phenomenon is also observed experimentally in the work of Balsara et. al[43], where they report the presence of hexagonal order but see no micron sized grains during the early stages of

ordering by spinodal decomposition. In fact, Balsara et al. observed an array of hexagonally packed, wormlike cylinders which were not stable and straightened out with time, much like what we see in our simulations (see Fig. 14). This suggests that the binary nanoparticle mixture indeed exhibits key features of BCP-like behavior, and that the proposed OPs would be able to track their disorder to order transitions.

3.2 Nucleation of the Alternating Gyroid Network

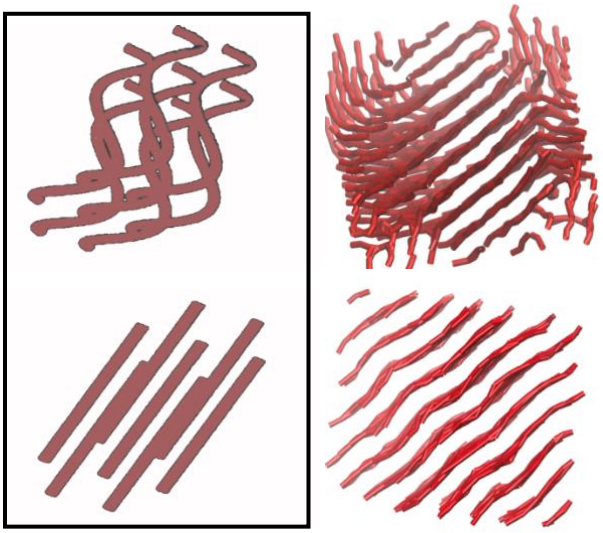

Figure 14: Left panel: Experimental observations of cylindrical order. Top: Wormlike cylinders that form during early stages of spinodal decomposition. Bottom: Fully aligned cylinders at the end of the ordering process. **Right panel:** Simulation snapshots showing a similar straightening out of minority component (X_A = 0.775) cylinders. Experimental image adapted from Ref. 30.

The growth of the alternating gyroid network from a disordered state at T = 300 K, X_A = 0.5 and ε_{AB} = 2.25 kcal/mol proceeds via nucleation and growth. A single ordered domain is seen to grow and propagate through the simulation box over time. Each network is evaluated separately using the proposed OP, but both are shown superimposed in Fig. 15, to demonstrate that these interpenetrated networks grow simultaneously from the isotropic liquid. To the best of our knowledge, there are no prior simulation studies that have developed an OP for the alternating gyroid network. Kumar and Molinero[62] demonstrated the use of certain bond OPs for BCP-like mesophases, however their analysis was limited to that of the double gyroid. The OP put forth in this paper depends only on the relative positions of the nodes, and hence serves as a good metric to not only understand the ordering mechanism of the alternating gyroid, but also as a basis for

future OPs of other network morphologies (most of which have nodes that lie on cubic lattices and can be described using spherical harmonics). To test the robustness of the OPs developed, we compared the fraction of ordered particles determined by each of the individual OPs

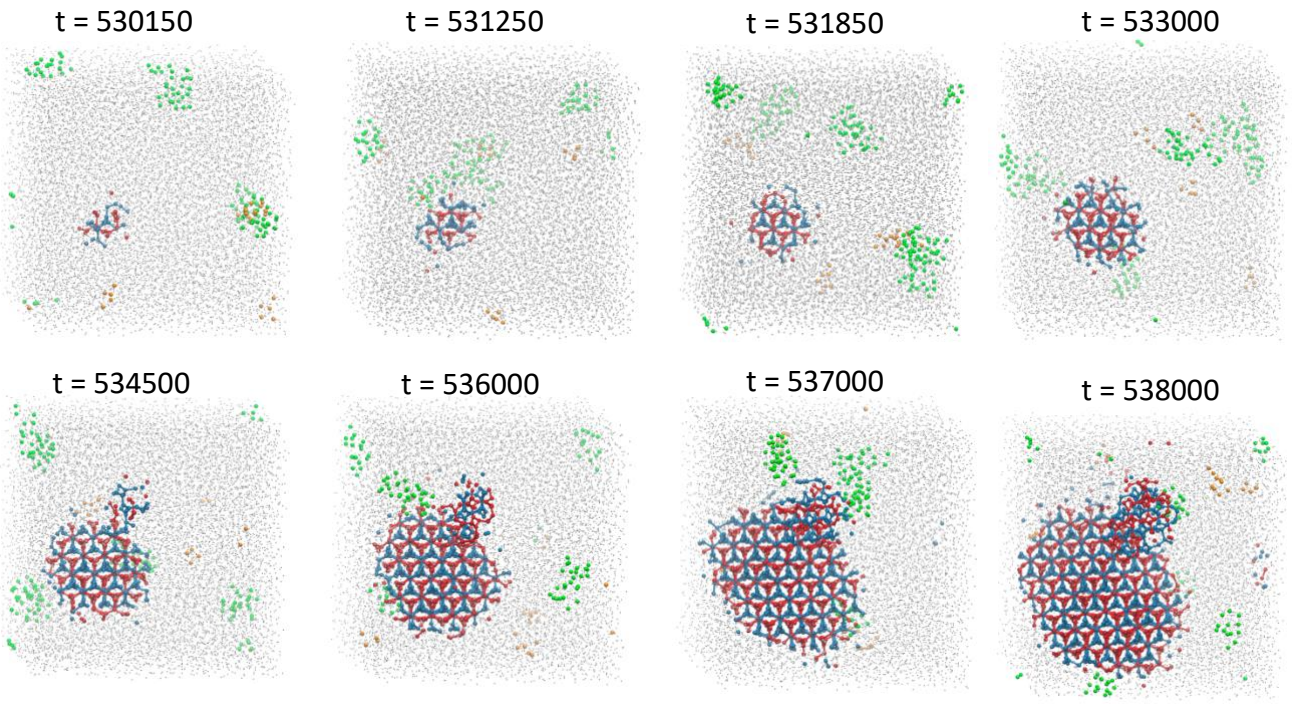

Figure 15: Nucleation and growth of the alternating gyroid phase at $X_A = 0.5$, $\varepsilon_{AB} = 2.25$ kcal/mol, $\sigma_{AB} = 1.02$, T = 300 K and P = 0 atm. The single ordered domain of the alternating gyroid is identified using the correlation function d_6 for each network separately. Red and blue correspond to the two interpenetrating networks that have been superimposed to show that they grow simultaneously from the isotropic liquid (colored in grey). The green and orange correspond to the particles that are identified to be "cylinder – like" and "lamellar – like" respectively, as detected by their corresponding OPs (only the four largest clusters are shown in each case). Time units are in fs.

(lamellar, cylinder and gyroid), at different times during the nucleation of the alternating gyroid from disorder. The results can be seen in Fig. 16 where both the lamellar and cylinder OPs predict a fairly constant low value as compared to the gyroid OP that steadily grows with time. The "lamellar – like" and "cylinder – like" particles detected by the corresponding OPs are also shown in Fig 15. It is clear that while the gyroid cluster grows steadily with time, the lamellar

and cylinder like particles are simply background fluctuations that do not form any contiguously ordered domain of significant size.

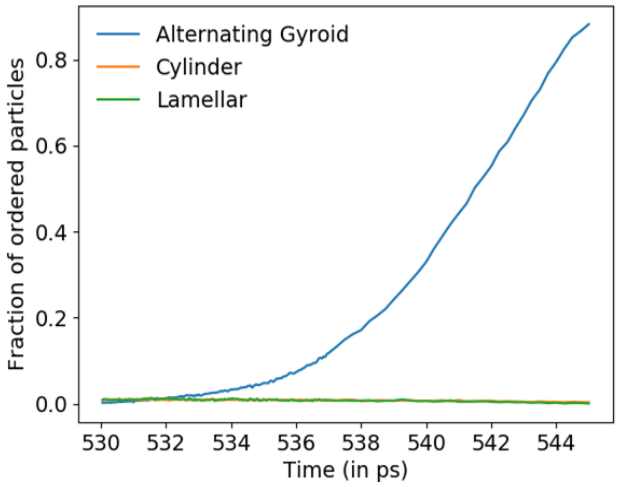

Figure 16: Fraction of ordered particles determined by each of the three OPs (lamellar, cylinder and gyroid) during the nucleation and growth of the alternating gyroid phase at $X_A = 0.5$, $\varepsilon_{AB} = 2.25$ kcal/mol, $\sigma_{AB} = 1.02$, T = 300K and P = 0 atm. The lamellar and cylinder OPs do not detect any cluster growth with time.

3.3 What if the outcome of the simulation is not known a-priori?

The OPs in this paper were designed having prior knowledge of the simulation outcome, or in other words the geometry of the putative ordered phase was known (either of lamellar, cylinder or alternating gyroid). Since this may not always be the case, it is imperative to put forth a framework that can iteratively search the simulation trajectory for possible motifs and track clusters based on all three OPs (or more), to see which one produces the largest number of ordered particles with time. The analysis would be similar to that shown in Fig. 16. Besides predicting the final phase, it could also reveal the presence of other transient competing phases that may form during the transition pathway.

4. Conclusions and Future Work

Table 1: Summary of the OPs developed for the lamellar, cylinder, and gyroid networks and the main steps involved in each. I. Identifying the characteristic signature vector for each phase, based on local geometries. II. Normalizing the signature vectors. III. Evaluating the vector components within an adequate neighbor cutoff. IV. Finding the correlation between signature vectors through an estimation of the appropriate dot product.

Name	Cylinder	Lamellar	Gyroid
I. Identify signature vectors	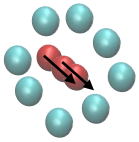	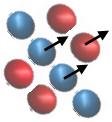	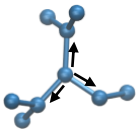
II. Normalizing the signature vectors	C.S. vector	L.S. vector	G.S. vector
III. Neighbor cutoff	First g(r) min	First g(r) min	Third g(r) min
IV. Correlation of Signature Vectors	Simple dot product	Simple dot product	Correlation Function – Eq. (2)

In this paper, we have implemented the binary nanoparticle mixture model developed by Kumar and Molinero[63], to study the ordering mechanism in lamellar, cylinder and alternating gyroid phases. This KM model forms BCP-like phases and allows the use of system sizes that can contain many more unit cells of the ordered morphology than is accessible through typical bead-spring type of polymer models. The large system sizes are especially useful for studies involving nucleation and growth, as we illustrate in this work.

While one can argue that the KM model used is not a suitable representation of BCPs, it does form phases that have similar geometries as BCPs, which is all that is needed for developing OPs that can detect the basic repeating motifs of those phases. Consequently, the OPs put forth depend only on the symmetry / relative arrangement of particles in the various phases (captured through dot products of the corresponding vectors), and upon slight modifications, it could also work for realistic BCP systems. For example, in a bead-spring type of BCP model, the center of mass of each block could play a role akin to each KM particle for the evaluation of OPs.

The proposed framework serves as the basis for our future work developing newer and more efficient OPs to characterize disorder to order transitions in BCPs. For example, the OP used for the lamellar phase could also be useful in detecting the formation of the perforated lamellar (PL) phase, since this OP relies on the presence of microphase segregated layers that are present in both phases. The interconnections between layers in the case of the PL may lead to non-contiguous ordered domains, which would serve to differentiate it from the lamellar phase. More generally, we hope to utilize the method used for the alternating gyroid technique toward other network morphologies such as the single diamond and plumbers' nightmare, whose nodes also lie on cubic lattices and could be resolved with the use of suitable bond orientation OPs. A summary of the OPs developed for the different morphologies is given in Table 1.

One of the main applications of the proposed OPs is complementary to employing them as reaction coordinates to extract free energy barriers and estimate nucleation rates using techniques such as umbrella sampling[60,61], forward flux sampling[74,75], metadynamics[59], and other similar rare-event sampling techniques. Such applications will allow us to ascertain how well our OPs can track the size of the largest ordered cluster, and be a good predictor of the committor probability[76] for studies on nucleation and growth.

5. References

1. Thorkelsson, K., Bai, P. & Xu, T. Self-assembly and applications of anisotropic nanomaterials : A review. *Nano Today* **10,** 48–66 (2015).
2. Boles, M. A., Engel, M. & Talapin, D. V. Self-Assembly of Colloidal Nanocrystals : From Intricate Structures to Functional Materials. *Chem. Rev.* **116,** (2016).
3. Stein, A., Wilson, B. E. & Rudisill, S. G. Design and functionality of colloidal-crystal-templated materials—chemical applications of inverse opals. *Chem. Soc. Rev.* **42,** 2763–2803 (2013).
4. Lin, Y., Boker, A. & He, J. Self-directed self-assembly of nanoparticle / copolymer

mixtures. *Nature* **434,** 55 (2005).

5. Hamley, I. W. *The Physics of Block Copolymers*. (Oxford University Press, 1998).
6. Feng, H., Lu, X., Wang, W., Kang, N.-G. & Mays, J. Block Copolymers: Synthesis, Self-Assembly, and Applications. *Polymers (Basel).* **9,** 494 (2017).
7. Zhou, M. *et al.* New type of membrane material for water desalination based on a cross-linked bicontinuous cubic lyotropic liquid crystal assembly. *J. Am. Chem. Soc.* **129,** 9574–9575 (2007).
8. Kibsgaard, J., Chen, Z., Reinecke, B. N. & Jaramillo, T. F. Engineering the surface structure of MoS 2 to preferentially expose active edge sites for electrocatalysis. *Nat. Mater.* **11,** 963–969 (2012).
9. Crossland, E. J. W. *et al.* A bicontinuous double gyroid hybrid solar cell. *Nano Lett.* **9,** 2807–2812 (2009).
10. Kimber, R. G. E., Walker, A. B., Schröder-Turk, G. E. & Cleaver, D. J. Bicontinuous minimal surface nanostructures for polymer blend solar cells. *Phys. Chem. Chem. Phys.* **12,** 844–851 (2010).
11. Docampo, P. *et al.* Triblock-terpolymer-directed self-assembly of mesoporous TiO 2 : High-performance photoanodes for solid-state dye-sensitized solar cells. *Adv. Energy Mater.* **2,** 676–682 (2012).
12. Cho, B.-K. Nanostructured organic electrolytes. *RSC Adv.* **4,** 395–405 (2014).
13. Patel, S. N., Javier, A. E. & Balsara, N. P. Electrochemically oxidized electronic and ionic conducting nanostructured block copolymers for lithium battery electrodes. *ACS Nano* **7,** 6056–6068 (2013).
14. Werner, J. G., Hoheisel, T. N. & Wiesner, U. Synthesis and characterization of gyroidal mesoporous carbons and carbon monoliths with tunable ultralarge pore size. *ACS Nano* **8,** 731–743 (2014).
15. Werner, J. G., Scherer, M. R. J., Steiner, U. & Wiesner, U. Gyroidal mesoporous multifunctional nanocomposites via atomic layer deposition. *Nanoscale* **6,** 8736–42 (2014).
16. Taylor, P. & Peters, B. Recent advances in transition path sampling : accurate reaction coordinates , likelihood maximisation and diffusive barrier-crossing dynamics. 37–41 (2010).

17. Wales, D. J. Perspective : Insight into reaction coordinates and dynamics from the potential energy landscape. **130901,** (2015).
18. Transtrum, M. K. *et al.* Perspective : Sloppiness and emergent theories in physics , biology , and beyond. *J. Chem. Phys.* **143,** (2015).
19. Sanz, E., Vega, C., Espinosa, J. R., Abascal, J. L. F. & Valeriani, C. Homogeneous ice nucleation at moderate supercooling from molecular simulation. *J. Am. Chem. Soc.* **135,** 15008–15017 (2013).
20. Reinhardt, A., Doye, J. P. K., Noya, E. G. & Vega, C. Local order parameters for use in driving homogeneous ice nucleation with all-atom models of water. *J. Chem. Phys.* **137,** 1–10 (2012).
21. Haji-akbari, A. & Debenedetti, P. G. Direct calculation of ice homogeneous nucleation rate for a molecular model of water. *PNAS* **112,** 10582–10588 (2015).
22. Barnes, B. C. *et al.* Two-component order parameter for quantifying clathrate hydrate nucleation and growth. *J. Chem. Phys.* **140,** (2014).
23. Barnes, B. C., Knott, B. C., Beckham, G. T., Wu, D. T. & Sum, A. K. Reaction Coordinate of Incipient Methane Clathrate Hydrate Nucleation. *J. Phys. Chem. B* **118,** 13236–13243 (2014).
24. Freiser, M. J. Ordered States of a Nematic Liquid. *Phys. Rev. Lett.* **24,** 1041–1043 (1970).
25. McMillan, W. L. Simple Molecular Model for the Smectic A Phase of Liquid Crystals. *Phys. Rev. A* **4,** 1238–1246 (1971).
26. Steinhardt, P. J., Nelson, D. R. & Ronchetti, M. Bond-orientational order in liquids and glasses. **28,** (1983).
27. Rein, P., Ruiz-montero, M. J. & Frenkel, D. Numerical calculation of the rate of crystal nucleation in a Lennard-Jones system at moderate undercooling. *J. Chem. Phys.* **104,** 9932–9947 (1996).
28. Lechner, W. & Dellago, C. Accurate determination of crystal structures based on averaged local bond order parameters. *J. Chem. Phys.* **129,** (2008).
29. Crocker, J. & Grier, D. Methods of Digital Video Microscopy for Colloidal Studies. *J. Colloid Interface Sci.* **179,** 298–310 (1996).
30. Weeks, E. R., Crocker, J.-C., Levitt, A. C., Schofield, A. & Weitz, D. A. Three-Dimensional Direct Imaging of Structural Relaxation Near the Colloidal Glass Transition.

Science (80-.). **287,** 627 (2000).

31. Varadan, P. & Solomon, M. J. Direct visualization of long-range heterogeneous structure in dense colloidal gels. *Langmuir* **19,** 509–512 (2003).
32. Veltkamp, R. C. & Hagedoorn, M. State of the Art in Shape Matching. in *Principles of Visual Information Retrieval* (ed. Lew, M. S.) 87–119 (Springer, London, 2001).
33. Lu, X., Colbry, D. & Jain, A. K. Three-Dimensional Model Based Face Recognition. *Proc ICPR* **1,** 362–366 (2004).
34. Harkless, C. R., Singh, M. A., Nagler, S. E., Stephenson, G. B. & Jordan-Sweet, J. L. Small-angle x-ray-scattering study of ordering kinetics in a block copolymer. *Phys. Rev. Lett.* **64,** 2285–2288 (1990).
35. Hashimoto, T., Kowsaka, K., Shibayama, M. & Suehiro, S. Time-Resolved Small-Angle X-ray Scattering Studies on the Kinetics of the Order-Disorder Transition of Block Polymers. 1. Experimental Technique. *Macromolecules* **19,** 750–754 (1986).
36. Stühn, B., Vilesov, A. & Zachmann, H. G. Structure Relaxation and Metastable States at the Microphase Separation Transition in Diblock Copolymers: Experiments with Time-Resolved Small-Angle X-ray Scattering. *Macromolecules* **27,** 3560–3565 (1994).
37. Fredrickson, G. H. & Helfand, E. Fluctuation effects in the theory of microphase separation in block copolymers. *J. Chem. Phys.* **87,** (1987).
38. Fredrickson, G. H. & Binder, K. Kinetics of metastable states in block copolymer melts. *J. Chem. Phys.* **91,** 7265 (1989).
39. Hashimoto, T. & Sakamoto, N. Nucleation and Anisotropic Growth of Lamellar Microdomains in Block Copolymers. *Macromolecules* **28,** 4779–4781 (1995).
40. Hashimoto, T., Sakamoto, N. & Koga, T. Nucleation and growth of anisotropic grain in block copolymers near order-disorder transition. *Phys. Rev. E - Stat. Physics, Plasmas, Fluids, Relat. Interdiscip. Top.* **54,** 5832–5835 (1996).
41. Dai, H. J., Balsara, N. P., Garetz, B. A. & Newstein, M. C. Grain growth and defect annihilation in block copolymers. *Phys. Rev. Lett.* **77,** 3677–3680 (1996).
42. Balsara, N. P. *et al.* Identification of the molecular parameters that govern ordering kinetics in a block copolymer melt. *Macromolecules* **31,** 5309–5315 (1998).
43. Balsara, N. P., Garetz, B. A., Newstein, M. C., Bauer, B. J. & Prosa, T. J. Evolution of microstructure in the liquid and crystal directions in a quenched block copolymer melt.

Macromolecules **31,** 7668–7675 (1998).

44. Hohenberg, P. C. & Swift, J. B. Metastability in fluctuation driven first-order transitions: Nucleation of lamellar phases. *Phys. Rev. E* **52,** 1828–1845 (1995).
45. Fredrickson, G. H., Ganesan, V. & Drolet, F. Field-theoretic computer simulation methods for polymers and complex fluids. *Macromolecules* **35,** 16–39 (2002).
46. Alexander-Katz, A. & Fredrickson, G. H. Diblock copolymer thin films: A field-theoretic simulation study. *Macromolecules* **40,** 4075–4087 (2007).
47. Fried, H. & Binder, K. The microphase separation transition in symmetric diblock copolymer melts: A Monte Carlo study. *J. Chem. Phys.* **94,** 8349–8366 (1991).
48. Vassiliev, O. N. & Matsen, M. W. Fluctuation effects in block copolymer melts. *J. Chem. Phys.* **118,** 7700–7713 (2003).
49. Matsen, M. W., Griffiths, G. H., Wickham, R. A. & Vassiliev, O. N. Monte Carlo phase diagram for diblock copolymer melts. *J. Chem. Phys.* **124,** (2006).
50. Zong, J. & Wang, Q. Fluctuation/correlation effects in symmetric diblock copolymers: On the order-disorder transition. *J. Chem. Phys.* **139,** (2013).
51. Detcheverry, F. A., Pike, D. Q., Nealey, P. F., Müller, M. & De Pablo, J. J. Monte Carlo simulation of coarse grain polymeric systems. *Phys. Rev. Lett.* **102,** 2–5 (2009).
52. Pike, D. Q., Detcheverry, F. A., Müller, M. & De Pablo, J. J. Theoretically informed coarse grain simulations of polymeric systems. *J. Chem. Phys.* **131,** (2009).
53. Groot, R. D., Madden, T. J., Dynamic simulation of diblock copolymer microphase separation *J. Chem. Phys.* **108,** (1998).
54. Sandhu, P., Zong, J., Yang, D. & Wang, Q. On the comparisons between dissipative particle dynamics simulations and self-consistent field calculations of diblock copolymer microphase separation. *J. Chem. Phys.* **138,** (2013).
55. Gavrilov, A. A., Kudryavtsev, Y. V. & Chertovich, A. V. Phase diagrams of block copolymer melts by dissipative particle dynamics simulations. *J. Chem. Phys.* **139,** (2013).
56. Glaser, J., Medapuram, P., Beardsley, T. M., Matsen, M. W. & Morse, D. C. Universality of block copolymer melts. *Phys. Rev. Lett.* **113,** 1–5 (2014).
57. Medapuram, P., Glaser, J. & Morse, D. C. Universal phenomenology of symmetric diblock copolymers near the order-disorder transition. *Macromolecules* **48,** 819–839 (2015).

58. Carilli, M. F., Delaney, K. T. & Fredrickson, G. H. Nucleation of the lamellar phase from the disordered phase of the renormalized Landau-Brazovskii model. *J. Chem. Phys.* **148,** (2018).
59. Barducci, A., Bonomi, M. & Parrinello, M. Metadynamics. *Wiley Interdiscip. Rev. Comput. Mol. Sci.* **1,** 826–843 (2011).
60. Auer, S. & Frenkel, D. Quantitative Prediction Of Crystal-Nucleation Rates For Spherical Colloids: A Computational Approach. *Annu. Rev. Phys. Chem.* **55,** 333–361 (2004).
61. Auer, S. & Frenkel, D. Numerical prediction of absolute crystallization rates in hard-sphere colloids. *J. Chem. Phys.* **120,** 3015–3029 (2004).
62. Kumar, A. & Molinero, V. Why Is Gyroid More Difficult to Nucleate from Disordered Liquids than Lamellar and Hexagonal Mesophases ? *J. Phys. Chem. B* **122,** 4758–4770 (2018).
63. Kumar, A. & Molinero, V. Self-Assembly of Mesophases from Nanoparticles. *J. Phys. Chem. Lett.* **8,** 5053–5058 (2017).
64. Martínez-Veracoechea, F. J. & Escobedo, F. A. Simulation of the gyroid phase in off-lattice models of pure diblock copolymer melts. *J. Chem. Phys.* **125,** 0–12 (2006).
65. Matsen, M. W. & Schick, M. Stable and Unstable Phases of a Diblock Copolymer Melt. *Phys. Rev. Lett.* **72,** 2660–2663 (1994).
66. Plimpton, S. Fast Parallel Algorithms for Short – Range Molecular Dynamics. *J. Comput. Phys.* **117,** 1–19 (1995).
67. Meuler, A. J., Hillmyer, M. A. & Bates, F. S. Ordered network mesostructures in block polymer materials. *Macromolecules* **42,** 7221–7250 (2009).
68. Khaderi, S. N., Deshpande, V. S. & Fleck, N. A. International Journal of Solids and Structures The stiffness and strength of the gyroid lattice. *Int. J. Solids Struct.* **51,** 3866–3877 (2014).
69. Saranathan, V., Osuji, C. O., Mochrie, S. G. J., Noh, H. & Narayanan, S. Crystals in Butterfly Wing Scales. *Proc. Natl. Acad. Sci. U. S. A.* **107,** 11676–11681 (2010).
70. Dolan, J. A. *et al.* Optical Properties of Gyroid Structured Materials: From Photonic Crystals to Metamaterials. *Adv. Opt. Mater.* **3,** 12–32 (2015).
71. Wu, L., Zhang, W. & Zhang, D. Engineering Gyroid-Structured Functional Materials via Templates Discovered in Nature and in the Lab. *Small* **11,** 5004–5022 (2015).

72. Sun, T., Tang, P., Qiu, F., Yang, Y. & Shi, A. C. Formation of Single Gyroid Nanostructure by Order–Order Phase Transition Path in ABC Triblock Terpolymers. *Macromol. Theory Simulations* **26,** 1–11 (2017).
73. Filion, L., Ni, R., Frenkel, D. & Dijkstra, M. Simulation of nucleation in almost hard-sphere colloids: The discrepancy between experiment and simulation persists. *J. Chem. Phys.* **134,** (2011).
74. Allen, R. J., Valeriani, C. & Rein, P. Forward flux sampling for rare event simulations. *J. Phys. Condens. Matter* **21,** (2009).
75. Borrero, E. E. & Escobedo, F. A. Reaction coordinates and transition pathways of rare events via forward flux sampling. *J. Chem. Phys.* **127,** (2007).
76. Beckham, G. T. & Peters, B. Optimizing nucleus size metrics for liquid-solid nucleation from transition paths of near-nanosecond duration. *J. Phys. Chem. Lett.* **2,** 1133–1138 (2011).

CHAPTER 2

Application of Local Order Parameters to Oligomeric and Polymeric Systems

1. Introduction

Block copolymers (BCP) exhibit a rich phase behavior and have been studied extensively over the years to understand the factors that control their self-assembly. For linear diblock copolymers (dBCP), for example, the strength of the incompatibility between blocks and their relative volume fractions are key characteristics that determine the tendency of these molecules to undergo a "disorder to order" transition. The disordered state lacks any kind of discernible long-range structural order, such as layers (lamellar phase), cylinders (hexagonal phase), or interwoven networks (gyroid phase). Nanoscopic domains having certain short-range order or geometric motifs nucleate and grow as the system travels along the transition pathway towards the ordered state. Key to tracking this transition is the availability of a good "order parameter" (OP), a metric that quantifies the degree of order in the system[1,2].

In Chapter 1, we discussed the need for a local OP based on geometric considerations, that can be used in techniques like metadynamics[3] or umbrella sampling[4,5], to extract free energy barriers. We further used the KM model[6] to access large system sizes, and develop OPs for three of the BCP phases (lamellar, cylinder and alternating gyroid). While the KM model served as a good platform to test our OPs, we had yet to confirm their validity as a suitable OP for more "realistic" simulation models of BCPs.

In this Chapter, we attempt to apply our OPs from Chapter 1 to study the disorder-to-order transition of two polyphilic polymeric systems of practical importance: (i) the isotropic-to-lamellar phase transition in a symmetric dBCP simulated via dissipative particle dynamics (DPD)[7], and (ii) the isotropic-to-single diamond (D1) phase transition in a bolaamphiphile

system simulated via molecular dynamics. Unlike the systems studied in Chapter 1 which have yet to be realized experimentally, the systems studied here have been well characterized in experiments[8,9] and in previous theoretical and simulation studies[10–14]. Both applications entail distinct modifications to the OPs from Chapter 1 and illustrate how such a framework can be extended to more complex systems. In particular, the lamellar dBCP system serves to illustrate how to "coarsen" the particle coordinates of multiatomic linear molecules into a minimalistic pseudo-center representation that can be mapped into a KM-like description. The bolaamphiphile system further illustrates how to extend the methodology developed for the gyroid network in Chapter 1 to a relatively novel network phase (D1), formed by a molecule containing 3 types of chemical blocks (i.e., a triblock co-oligomer) and a branched (a "T-shaped bola") structure. By demonstrating the use of our OPs in two different simulation models (of polymers and bolaamphiphiles), we hope to illustrate their usefulness as a reaction coordinate for studies aimed at understanding order-disorder kinetic pathways in BCP or similar systems.

2. Formation of the Lamellar Phase via Dissipative Particle Dynamics

One of the simplest morphologies formed by dBCPs is the lamellar phase consisting of alternating layers of two blocks (A and B). Several computational studies have used a highly coarse-grained soft-bead, mesoscale model typically associated with dissipative particle dynamics (DPD) to described the phase behavior of dBCPs and to analyze the disorder to order transition in the lamellar phase[12,15,13]. Here, we use the model to form the lamellar phase and apply our OP to track its transition from a disordered state.

2.1 Model Details

In the DPD model, polymers are represented as chains of soft beads and springs, where each bead represents a segment of a polymer chain that moves according to Newton's equations

of motion. The total force on a bead is given by the sum of the conservative F^C, random F^R, and frictional F^D (dissipative) forces[7]. Each bead interacts with all other beads through the conservative force:

$$F_{ij}^{C} = \begin{cases} a_{ij}(1 - r_{ij})\hat{r_{ij}} & (r_{ij} < 1) \\ 0 & (r_{ij} \geq 1) \end{cases} \qquad (1)$$

where a_{ij} represents the strength of repulsion. Note that Eq. (1) implies that the "diameter" of a soft bead (where repulsion goes to zero) is unity and provides the reference length used in expressing various properties. All parameters are reported in reduced units. Beads of the same type interact with $a_{ii} = 25$ while for different-type beads $a_{ij} = a_{ii} + 3.27\chi$, where χ is the Flory - Huggins interaction parameter used to quantify the degree of segregation between different blocks. It is this dependence on χ that allows a coarse-grained model like DPD to capture the main energetic disparity between blocks and provide for experimental values of χ to be incorporated into simulations. The beads are connected through a harmonic potential force:

$$F_{ij}^{har} = -k_h r_{ij} \hat{r_{ij}} \qquad (2)$$

where $k_h = 4$ is the spring constant used. The system is simulated at a number density = 3 and box length $L_{box} = 21$ to represent melt conditions. Each chain consists of 8 beads (N), 4 from each block ($f = 0.5$) and χN is chosen to be 40 in accordance with the DPD phase diagram[16] ($\chi N_{ODT} \approx 28$ for $f = 0.5$). The integration timestep used is $\Delta t^* = 0.05$, and simulations are run for 5×10^6 steps to ensure equilibration.

2.2 Mapping Structure into Coarse-grained Pseudo-Center Model

The lamellar phase shown in Fig. 1a consists of approximately 5.0σ thick layers of alternating A and B domains, where σ is a characteristic length scale of the model roughly equal to the diameter of a bead in the dBCP molecule. This is in contrast to the single particle thick

domains obtained in the KM model, which could be thought of as representing the centers of a thicker domain. Since our OP essentially tracks cluster growth based on these domain "centers", one approach to map the current DPD lamellar structure into a reduced, but equivalent KM-like lamellar structure, is to identify surrogate bead "centers" in each layer. In this way, a DPD lamella is converted into a form that can be "directly" used by our OP. We do this in a two-step process. In the first step, each block is replaced by a pseudo-block point located at the blocks' center of mass (Fig. 1b). At this point each lamella layer is roughly two pseudo-blocks thick. To try to reduce this thickness even more, in the second step, each pseudo-block is paired to the closest pseudo-block of the same block type, but one that does not share the same interface, i.e., the distance between their respective interface beads (first bead of the other block) should be greater than a critical value l_c. This value is taken to be l_c = 5.0, considering that the distance between interface beads of neighboring chains that do not share the same interface, would be on the order of the average lamellar thickness ≈ 5.5 - 6.0 (see Fig. 2). These pairs are then replaced

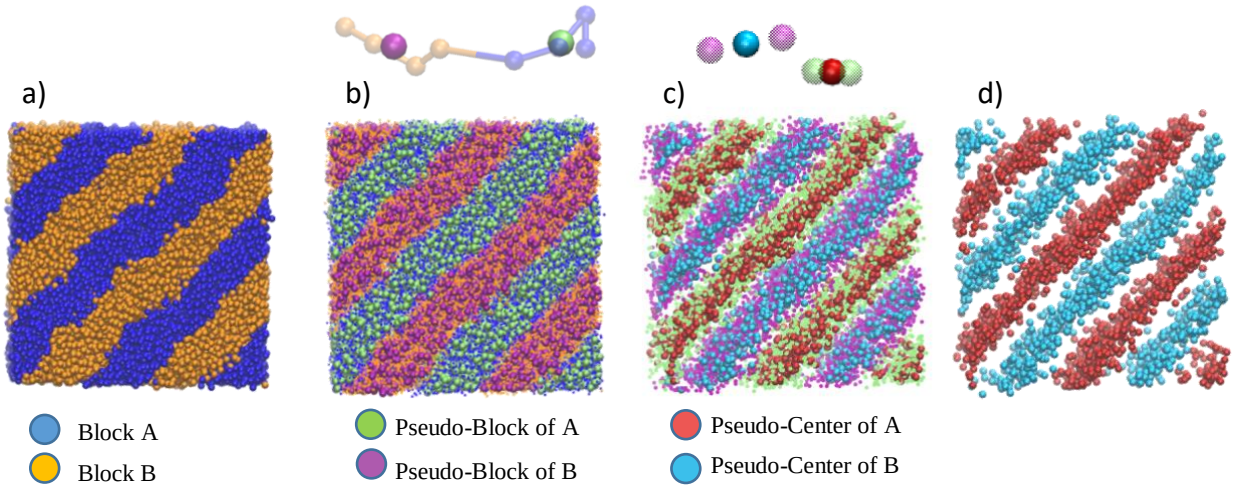

Figure 1: Snapshots of the lamellar phase obtained using the dBCP DPD model at f = 0.5, χN=40 and L_{box}=21. a) Original structure showing the multibead-thick layered domains. b) Top: Replacing chains with pseudo-blocks at block centers' of mass (COM). Bottom: Snapshot showing the original beads and the identified pseudo-blocks. c) Top: Pairing nearest neighbor pseudo-blocks that don't share the same interface and identifying pseudo-centers at the pair's COM. Bottom: Snapshot showing the pseudo-blocks and pseudo-centers. d) Final reduced structure obtained with pseudo-centers.

by a set of "pseudo-centers" located at the pseudo-block pairs' center of mass (Fig. 1c). Iterating over all chains, we obtain the reduced form of the structure, as an attempt to approximately map the domain centers via pseudo-centers (Fig. 1d). This reduced structure is used in all further calculations. The results are only slightly sensitive to l_c, and any value within the range of 4.5 to 6.0 would work sufficiently well to differentiate between the chains.

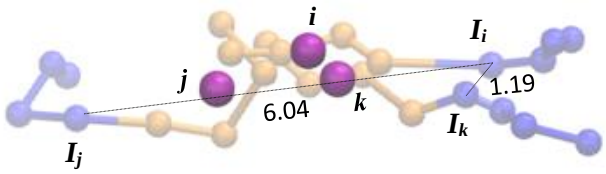

Figure 2: Criteria for selecting l_c – Distance between interface beads (denoted as I_x) of neighboring chains that do not share the same interface (6.04) > those that share the same interface (1.19). Pseudo-block *i* is hence paired to pseudo-block *j* and not *k*. Coloring scheme same as Fig.1.

2.3 Growth of the Lamellar Phase

The system is first allowed to equilibrate for 10^6 timesteps at $\chi N = 25$, $f = 0.5$, corresponding to the isotropic region of the phase diagram. The final configuration obtained is then used as a starting point and subjected to an instantaneous jump to the desired χN of 40. The growth of the lamellar phase from disorder is tracked using a procedure similar to that described in Section 2.3.1 of Chapter 1 for the lamellar phase. Particles here refer to the pseudo-centers.

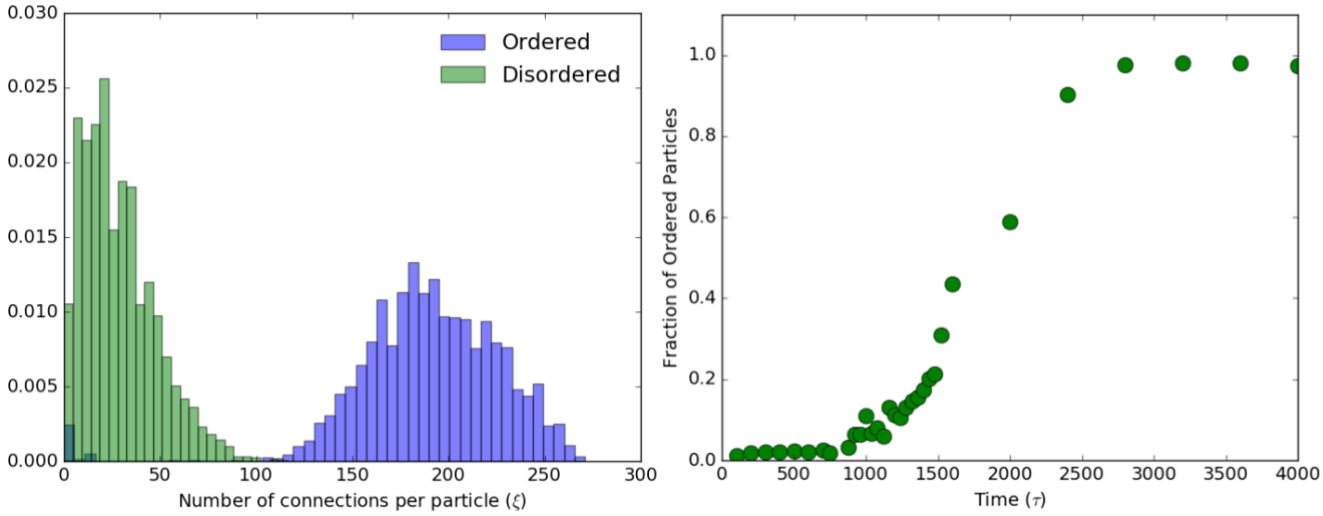

Figure 3: Left - Distribution function of the number of connections per particle for the lamellar phase (DPD model). Two particles are connected if the dot product of their LS vectors is greater than 0.95. **Right –** Plot showing the growth of the ordered phase with time.

For every particle *i*, a cutoff radius (r_c) is defined within which, all particles of the same type are identified as "nearest neighbors". Here, r_c is chosen to be 5.0 (equal to the first minimum in the pair radial distribution function of pseudo-centers) and a value large enough to get a good planar fit. The "neighbor" particles are used to fit a plane and identify the direction of the normal vector to the plane, denoted as the lamella-signature "LS" vector of particle *i*. The process is repeated until each particle has its own LS vector. To quantify the degree of alignment, the angle between neighboring LS vectors is measured through their dot product. If the dot product exceeds 0.95, the two particles are said to be connected. Figure 3 shows the histograms of the number of connections per particle for the disordered and ordered cases. From Fig. 3 we define a threshold of $\xi > 80$, to determine if a particle is "lamellar-like". This allows us to identify all the ordered particles, after which they are clustered depending on their proximity to one another using a cutoff of r_c and tracked with time (Fig. 4). The growth of the ordered particles with time is shown in Fig. 3, where the transition can be seen to be weakly first order, in agreement with experimental and theoretical studies on the disorder to lamellar transition[17,18]. Since the lamellar phase has unusually small nucleation barriers[19], and our degree of supercooling is high, we do not observe growth via nucleation of a single ordered domain. Instead we see the presence of multiple grains in the box that come together and align with time.

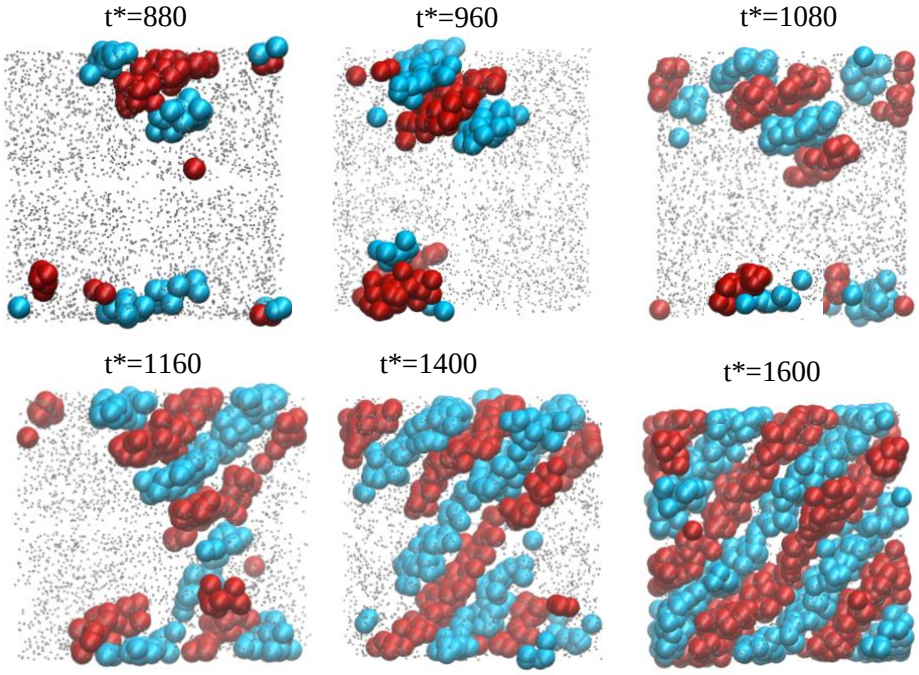

Figure 4: Growth of the lamellar phase at f = 0.5, χN=40 and L_{box} = 21. Red and blue correspond to the ordered A and B particles (or pseudo-centers) of the diblock copolymer, that grows from the isotropic liquid (colored in grey). Time is reported in reduced units

3. Formation of the "Single" Diamond in Bolaamphiphiles

Bolaamphiphiles are a class of molecules that consist of a hydrophobic backbone (e.g., a polyphenyl core) with two hydrophilic end groups (e.g., polar diol groups). Of these, the T-shaped bolaamphiphiles (TBA) also include a third segment consisting of a laterally attached flexible chain (e.g., alkyl or fluoroalkyl chains)[20,21]. The incompatibility between segments allows these molecules to self-assemble into a variety of different morphologies that can be tuned through changes in temperature and lateral chain length and design. A recent simulation study by Sun et al., confirmed the rich phase behavior exhibited by TBA, where they observed the formation of the "single" diamond (D1) and the "single" plumbers' nightmare (P1) phases, along with other more commonly observed morphologies[14]. Here, we attempt to use the principles that govern our OPs to detect the growth of the D1 phase from disorder. This D1 phase, as originally predicted by the Sun et al. simulation study, has also been experimentally

realized[22]. We adapt the methodology used for the alternating gyroid network (that lies on a BCC lattice) in Chapter 1, which we find particularly useful, since the D1 phase also lies on a cubic lattice but involves a different lattice symmetry (FCC).

3.1 Model Details

The model implemented by Sun et al. in Ref. [14] was adopted to simulate a system of 2700 TBA molecules, with a chain length of 6 (N_{rigid}) and 11 (N_{flx}) beads for the rigid backbone and flexible lateral chain respectively (see Fig. 5). Unlike the soft-beads used in the DPD model, here beads interact via a Lennard-Jones type of potential and hence represent a more detailed (less coarse-grained) representation of the molecules. All parameters are reported in reduced units. MD simulations were performed using the LAMMPS software[23], and forces were integrated using the Velocity Verlet algorithm with an integration step size of $\Delta t^* = 0.005$. The simulations were conducted in an NVT ensemble at a constant number density $\eta = 0.45$, and a temperature $T^*=1.05$ (using the Nose-Hoover thermostat). The conditions we chose are relatively close to the transition point, since the system disorders for $T^* > 1.1$, hence indicating a small supercooling. Under these conditions, we obtain the "single" diamond phase as shown in Fig. 6. This structure was converted into its equivalent skeleton form using the network analysis mentioned in Ref. [14], where each strut is a cluster of the blue beads (i.e. the hydrophobic backbone) and each node is a cluster of the red beads (i.e. the hydrophilic end groups). Note that the skeleton representation approach of Ref. [14] plays a similar role to the structure reduction approach we described to map the DPD lamella phase into pseudo-centers in section 2.2. For example, in the D1 phase the roughly spherical symmetry of a node allows the use of the center of mass of all beads making up that node as a single pseudo-bead, to be henceforth denoted as a pseudo-node. This gives us an ordered state node size distribution that consists of an average of

20-30 beads per node. In the disordered state, where there is no coherent network structure, only those clusters that lie within the node size distribution are defined to be nodes.

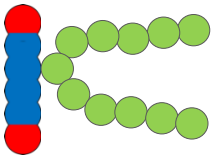

Figure 5: Schematic of the TBA molecule for N_{flx} = 11 and N_{rigid} = 6. Red beads correspond to the hydrophilic end groups; Blue beads correspond to the linear hydrophobic chain; Green beads correspond to the grafted flexible lateral chain.

3.2 Order parameter for the Single Diamond phase

In section 2.3.2 of Chapter 1, we saw that the symmetry of a cubic phase can be captured using vectors described by a set of spherical harmonic functions. Here we extend that idea to develop an OP for the D1 phase, whose nodes lie on a diamond cubic lattice having FCC symmetry. All further analysis involved only the position of the pseudo-nodes, which were obtained from the skeleton form shown in Fig. 6.

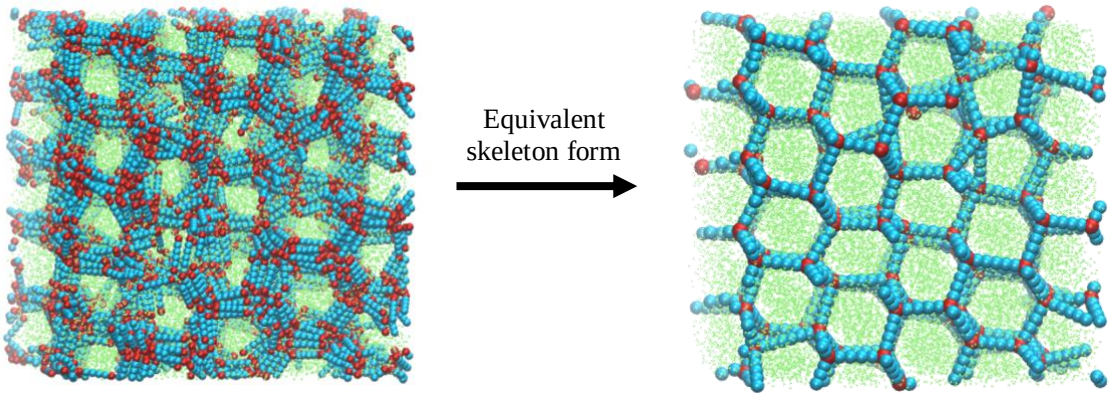

Figure 6: Left - Simulated snapshot of the "single" diamond (D1) phase consisting of 2700 molecules, obtained at T^*=1.05, η = 0.45, N_{flx} = 11 and N_{rigid} = 6. The red and blue correspond to the rigid backbone of the TBA that forms the D1 phase, with the red representing the hydrophilic end groups (that constitute the nodes), and blue representing the hydrophobic chain (that constitute the struts). Green represents the flexible lateral chain that forms the continuous phase. **Right** – Equivalent skeleton model (consisting of pseudo-nodes and struts) obtained after clustering and reducing nodal clusters into single beads.

These coordinates were used to compute the bond OPs described by Eq. (1)

$$q_{l,m}(i) = \frac{1}{N_b(i)} \sum_{j=1}^{l} Y_{l,m}(\theta_{i,j}, \phi_{i,j}) \qquad (3)$$

where $Y_{l,m}(\theta_{i,j}, \phi_{i,j})$ are the spherical harmonics, $m \in [-l, l]$ and $\theta_{i,j}$ and $\phi_{i,j}$ are the polar and

azimuthal angles of $r_{i,j}$ (distance vector between pseudo-nodes *i* and *j*) and r_i (position vector of pseudo-node *i*). $N_b(i)$ denotes the total number of neighbors for every pseudo-node, found within a cutoff distance r_c = the first g(r) minimum. The symmetry index *l* is chosen to be 4, after comparing the distributions of the q_6 and q_4 correlation functions, computed using Eq. (2) for all pairs of neighboring pseudo-nodes, in both the ordered and disordered cases (see Fig. 7a-f).

$$d_l(i,j) = \frac{\sum_{m=-l}^{l} q_{l,m}(i) q_{l,m}^*(j)}{\left(\sum_{m=-l}^{l} |q_{l,m}(i)|^2\right)^{1/2} \left(\sum_{m=-l}^{l} |q_{l,m}(j)|^2\right)^{1/2}} \quad (4)$$

Here * indicates the complex conjugate. While the distributions for the two phases overlap significantly for d_6 (Fig. 7a), they are better separated for d_4 (Fig. 7b).

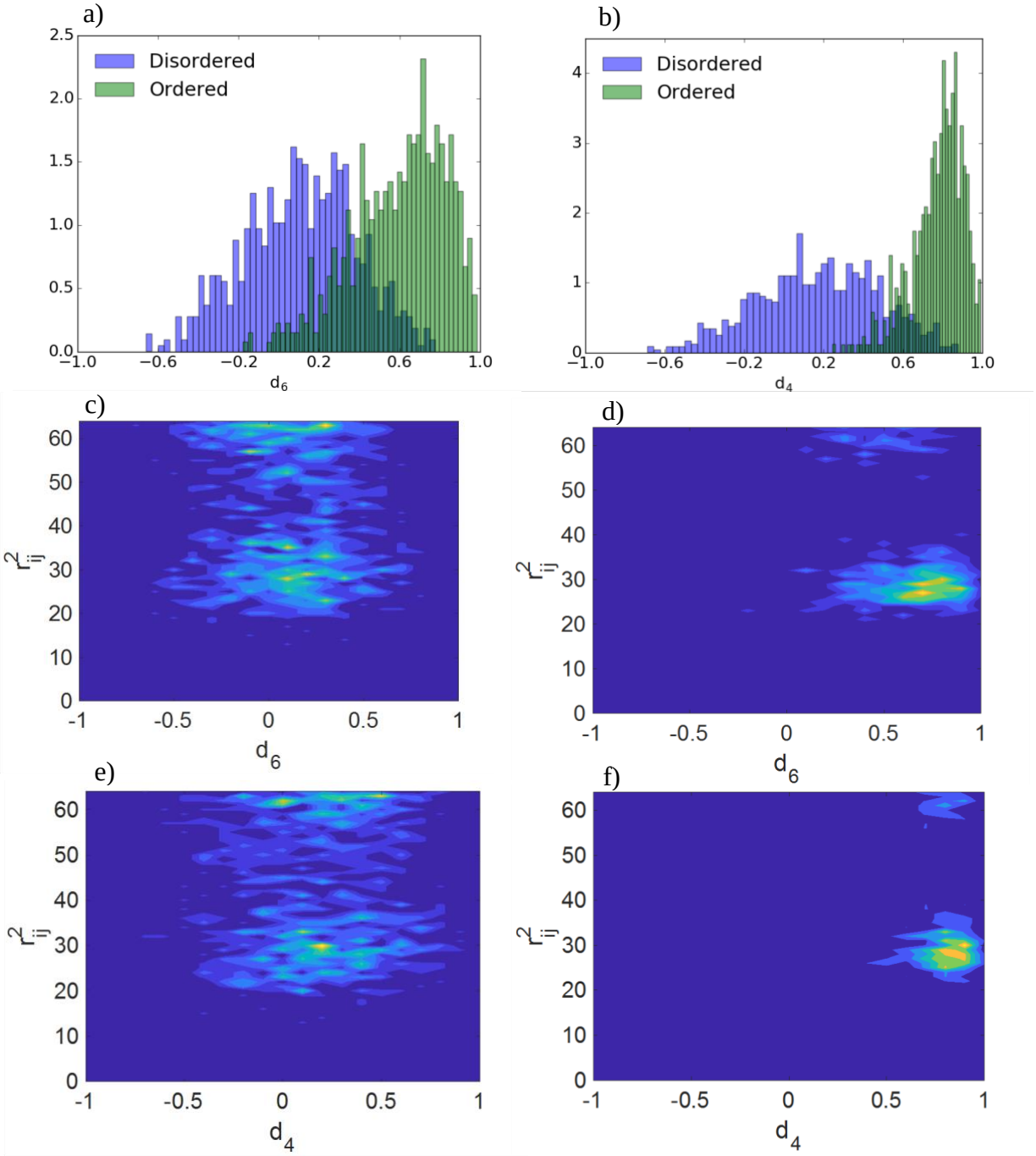

Figure 7: Histograms of the correlation functions d_6 and d_4 for the ordered and disordered phases of the "single" diamond of TBAs at T^*=1.05, η = 0.45, N_{flx} = 11 and N_{rigid} = 6. a) d_6 distributions showing significant overlap. b) d_4 distributions showing significant separation, suggesting a discriminating threshold of $d_4 > 0.66$. c-d) Two-dimensional histograms of d_6 with r_{ij}^2 for disordered and ordered phases, respectively. e-f) Two-dimensional histograms of d_4 with r_{ij}^2 for disordered and ordered phases, respectively.

The same can also be observed in the corresponding 2-D histograms of the ordered phase based on d_6 (Fig. 7d) and d_4 (Fig. 7f), with the former being significantly more diffuse than the latter. This confirms that the choice of symmetry index 4 is more discriminating. We can then define two neighboring pseudo-nodes to be connected if their d_4 value is larger than a threshold value $d_{4,c}$, i.e., $d_4 > d_{4,c} = 0.66$. Using this definition, we can effectively identify all the ordered pseudo-nodes, however we need to check how many such connections exist per pseudo-node for both the ordered and disordered phases. Fig. 8 shows the distribution function for the number of connections per pseudo-node, denoted by ξ. From this, we can define another threshold ξ_c to unambiguously identify "diamond-like" pseudo-nodes so that for $\xi(i) > \xi_c$ pseudo-node *i* is

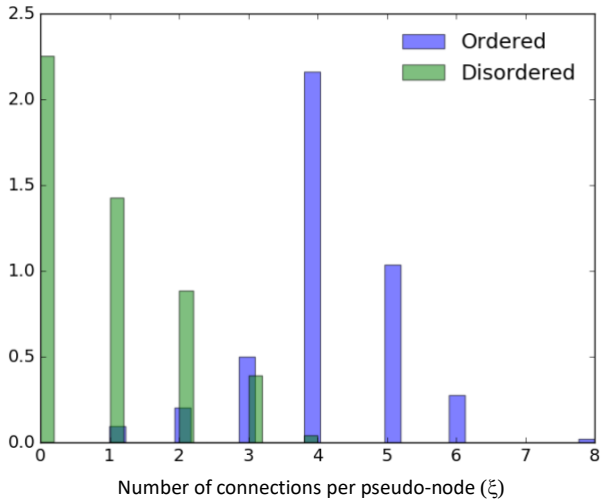

Figure 8: Distribution function of the number of connections per pseudo-node for the D1 phase. Two pseudo-nodes are considered connected if their correlation function d_4 is greater than 0.66.

considered "diamond-like", while for $\xi(i) \leq \xi_c$ it is considered to be "liquid-like". Based on the distributions shown in Fig. 8, ξ_c was set as 3. Using this criterion, the selection process is carried out until all the "diamond-like" pseudo-nodes have been identified. These pseudo-nodes are then clustered depending on their spatial proximity to one another, using the cutoff r_c. This allowed us to track the growth of the D1 phase from a disordered state. The ordered domain formed by the rigid rods can be seen to nucleate and grow with time in Fig. 9. The bolaamphiphile results

further support our hypothesis that order – disorder transitions in network morphologies can be mapped by identifying and tracking the pseudo-node positions alone, provided the final structure lies on a cubic lattice with well-defined symmetry.

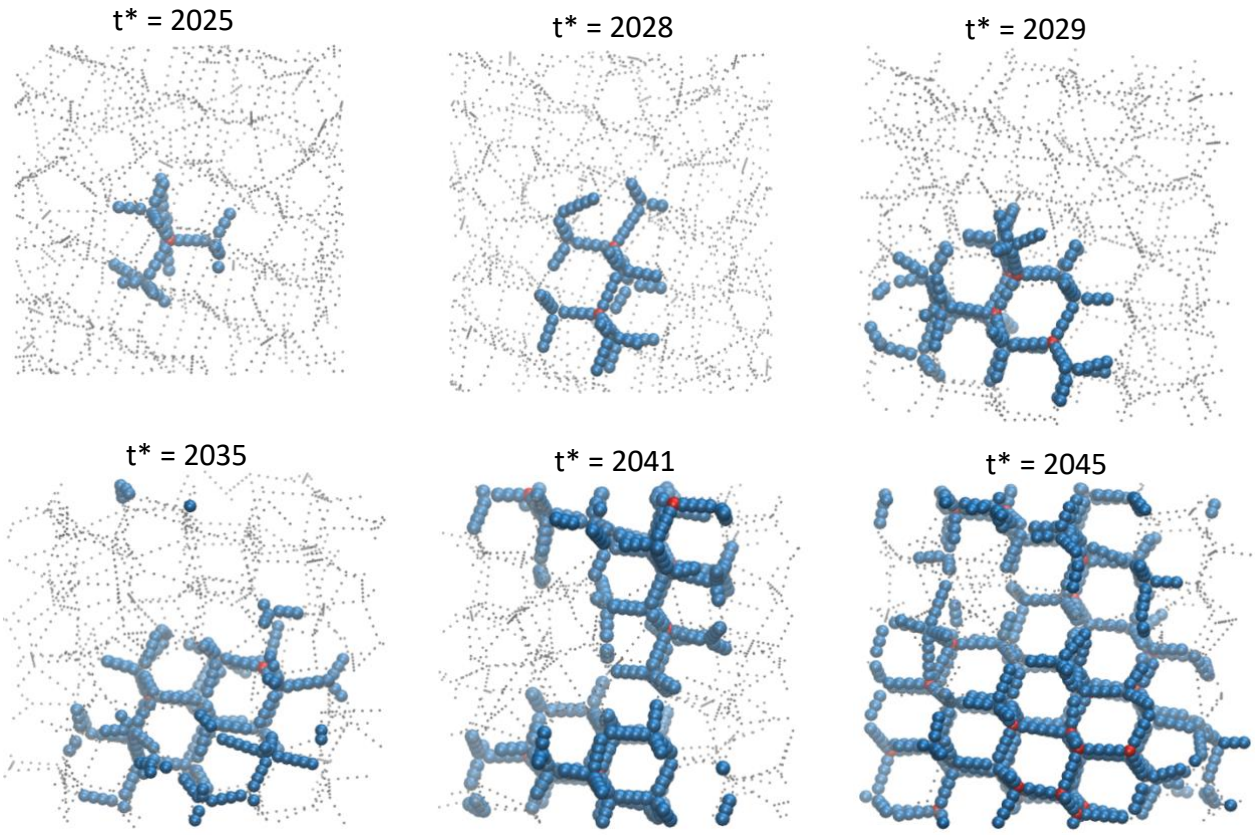

Figure 9: Growth of the D1 phase of TBAs at T^*=1.05, η = 0.45, N_{flx} = 11 and N_{rigid} = 6. The ordered domain is identified using the correlation function d_4 for the pseudo-nodes. Red and blue correspond to the pseudo-nodes and struts of the D1 phase, that grows from the isotropic liquid (colored in grey). For clarity, only the rigid rods are shown. Time is reported in reduced units (t^*/1000).

4. Conclusion

In this paper, we have implemented the local OPs developed in Chapter 1, toward more complex polymeric or oligomeric molecular models, namely, of linear diblock copolymers and of T-shaped bolaamphiphiles. The OPs are based on the description of domain "centers" of the different phases; i.e., the centers of individual layers in the lamellar phase, the axis of cylinders in the hexagonal phase, or the centers of mass of nodes in the gyroid network. Hence, to be able

to use our OP for the lamellar phase consisting of multi-particle-thick domains, we needed to convert it into a suitable single-particle-thick form. By doing so, we showed that we can effectively track the growth of the lamellar phase from a disordered state.

We also extended the method developed for the alternating gyroid toward another network morphology, the "single" diamond phase obtained via the self-assembly of T-shaped bolaamphiphile molecules. In this case, each nodal cluster characteristic of this phase can be readily reduced to a single domain center or nodal point. Since the nodes of the diamond phase are arranged in an FCC cubic lattice, we showed that the symmetry of any FCC-like motif was readily identified with the help of a bond orientational OP.

Both of these applications confirm the use of the OPs we proposed in Chapter 1 as effective metrics to track the evolution of systems undergoing disorder to order transitions. The underlying principle is the same: Identify the characteristic symmetry of the phase by analysis of the "finite elements" making up the domain centers and represent it through a set of appropriate vectors. The correlation between vectors then gives us the spatial extent of order in the system. An interesting observation regarding the choice of neighbor cutoff (r_c) used for our OPs was that it was of the order of the characteristic repeat-unit domain width or "period length" of the phase. For example, r_c for the lamellar phase was approximately equal to the lamella spacing i.e. the first g(r) minimum, irrespective of the model used (KM or DPD). For the gyroid, this translated to a longer distance to capture the proper "period length".

We intend to extend and develop this approach further, toward realistic molecular models of the cylinder phase and double gyroid phase seen in BCP, as well as employ them as reaction coordinates to extract free energy barriers and estimate nucleation rates using rare-event sampling techniques[3–5,24,25]. We also think the approach could work well for BCP models with

different bead diameters, as well as in surfactant-solvent systems or multicomponent BCP - homopolymer blends that exhibit complex phases and could be resolved with the help of our order parameters.

5. References

1. Taylor, P. & Peters, B. Recent advances in transition path sampling : accurate reaction coordinates , likelihood maximisation and diffusive barrier-crossing dynamics. 37–41 (2010).
2. Wales, D. J. Perspective : Insight into reaction coordinates and dynamics from the potential energy landscape. **130901,** (2015).
3. Barducci, A., Bonomi, M. & Parrinello, M. Metadynamics. *Wiley Interdiscip. Rev. Comput. Mol. Sci.* **1,** 826–843 (2011).
4. Auer, S. & Frenkel, D. Quantitative Prediction Of Crystal-Nucleation Rates For Spherical Colloids: A Computational Approach. *Annu. Rev. Phys. Chem.* **55,** 333–361 (2004).
5. Auer, S. & Frenkel, D. Numerical prediction of absolute crystallization rates in hard-sphere colloids. *J. Chem. Phys.* **120,** 3015–3029 (2004).
6. Kumar, A. & Molinero, V. Self - assembly of Mesophases from Nanoparticles. *J. Phys. Chem. Lett.* **8,** 5053–5058 (2017).
7. Groot, R. D. & Warren, P. B. Dissipative Particle Dynamics: Bridging the Gap between Atomistic and Mesoscopic Simulation. *J. Chem. Phys.* **107,** 4423 (1997).
8. Hashimoto, T. & Sakamoto, N. Nucleation and Anisotropic Growth of Lamellar Microdomains in Block Copolymers. *Macromolecules* **28,** 4779–4781 (1995).
9. Hashimoto, T., Sakamoto, N. & Koga, T. Nucleation and growth of anisotropic grain in block copolymers near order-disorder transition. *Phys. Rev. E* **54,** 5832–5835 (1996).
10. Carilli, M. F., Delaney, K. T. & Fredrickson, G. H. Nucleation of the lamellar phase from the disordered phase of the renormalized Landau-Brazovskii model. *J. Chem. Phys.* **148,** (2018).
11. Pike, D. Q., Detcheverry, F. A., Müller, M. & De Pablo, J. J. Theoretically informed coarse grain simulations of polymeric systems. *J. Chem. Phys.* **131,** (2009).
12. Groot, R. D. & Madden, T. J. Dynamic simulation of diblock copolymer microphase separation. *J. Chem. Phys.* **108,** (1998).

13. Gavrilov, A. A., Kudryavtsev, Y. V. & Chertovich, A. V. Phase diagrams of block copolymer melts by dissipative particle dynamics simulations. *J. Chem. Phys.* **139,** (2013).
14. Sun, Y., Padmanabhan, P., Misra, M. & Escobedo, F. A. Molecular dynamics simulation of thermotropic bolaamphiphiles with a swallow-tail lateral chain: formation of cubic network phases. *Soft Matter* **13,** 8542–8555 (2017).
15. Sandhu, P., Zong, J., Yang, D. & Wang, Q. On the comparisons between dissipative particle dynamics simulations and self-consistent field calculations of diblock copolymer microphase separation. *J. Chem. Phys.* **138,** (2013).
16. Martínez-Veracoechea, F. J. & Escobedo, F. A. Simulation of the gyroid phase in off-lattice models of pure diblock copolymer melts. *J. Chem. Phys.* **125,** 0–12 (2006).
17. Fredrickson, G. H., Helfand, E., Fredrickson, G. H. & Helfand, E. Fluctuation effects in the theory of microphase separation in block copolymers. *J. Chem. Phys.* **87,** (1987).
18. Lee, S., Gillard, T. M. & Bates, F. S. Fluctuations, Order and Disorder in Short Diblock Copolymers. *AIChe J.* **59,** 3–194 (2013).
19. Fredrickson, G. H. & Binder, K. Kinetics of metastable states in block copolymer melts. *J. Chem. Phys.* **91,** 7265 (1989).
20. Cheng, X. *et al.* Calamitic Bolaamphiphiles with (Semi) Perfluorinated Lateral Chains : Polyphilic Block Molecules with New Liquid Crystalline Phase Structures. **1,** 2057–2070 (2003).
21. Tschierske, C. Liquid crystal engineering – new complex mesophase structures and their relations to polymer morphologies , nanoscale patterning and crystal engineering. **15,** (2007).
22. Poppe, S., Prehm, M., Zeng, X., Ungar, G. & Tschierske, C. T-shaped bolapolyphiles with cubic LC phases. in *the 13th European Conference on Liquid Crystals, Manchester, UK, September* (2015).
23. Plimpton, S. Fast Parallel Algorithms for Short – Range Molecular Dynamics. *J. Comput. Phys.* **117,** 1–19 (1995).
24. Allen, R. J., Valeriani, C. & Rein, P. Forward flux sampling for rare event simulations. *J. Phys. Condens. Matter* **21,** (2009).
25. Borrero, E. E. & Escobedo, F. A. Reaction coordinates and transition pathways of rare events via forward flux sampling. *J. Chem. Phys.* **127,** (2007).